Bremen, July 12, 2019

Letter to the Editor of paper acp-2019-5

Dear Editor,

on behalf of all co-authors I have prepared this document, which provides the point-by-point responses to the reviews and a highlighting of all changes made in the revised manuscript.

Best regards,

Oliver Schneising
(corresponding author)

Final response to referee comments on paper acp-2019-5

First of all, we would like to thank both reviewers for their critical and constructive comments, which helped to significantly improve the manuscript. The concise letter-style of the manuscript was not fully adequate for the presentation of a new field of application of satellite data and was replaced by a more detailed edition with considerably extended analysis, discussion, and conclusions, in particular with respect to the associated uncertainties. We explicitly discuss and quantify uncertainties arising from boundary layer height, plume dynamics, and smoke aerosols in the revised version.

The data set providing the boundary layer heights was replaced by the ECMWF ERA5 reanalysis, which is available at hourly resolution. The previously used ECMWF analysis is only available at time steps of 6 hours (0, 6, 12, 18 UTC). Therefore, the maximum boundary layer height at local noon close to the time of the satellite overpass (21:30 UTC = 13:30 local time) was missed leading to underestimated heights. The usage of ERA5 provides far more realistic results. As a consequence, all city scenes, even the most polluted ones, likely comply with national ambient air quality standards, which is in line with isolated ground-based air quality measurements. The largest detected boundary layer concentration anomaly within all city radii (scene near Sacramento Airport on November 10) amounts now to $5.42\,\mathrm{mgCO\,m^{-3}}$ [3.97–5.96; 1σ].

We also prepared the companion paper amt-2019-243 (Schneising et al., 2019), which describes the underlying algorithm in detail and includes error characteristics based on synthetic data, validation of the satellite data with reference data, and comparisons to the operational product.

Below we give answers and clarifications to all comments made by the referees (repeated in italics).

Anonymous Referee #1

General comments

Reviewer: *The style of the text is at the edge of what is acceptable for scientific writing. It uses emotional and judgemental wording, (non-exhaustive) list of examples: title: "devastating"; abstract: "one of the most disastrous months in Californian history", "destructive wildfires raging", "burnt to cinders"; introduction: "the town of Paradise was wiped out", "an unprecedented instance in history"; conclusion: "The analysed fires were the latest episodes of the deadliest and most destructive wildfire season the state of California has ever faced." Most of these statements can be removed without loss of any information.*

Authors: We agree with the reviewer and changed the style of the text at the passages in question but retained the description of the statistics of the California Department of Forestry and Fire Protection, e.g., that the wildfire season 2018 has been the most destructive on record with respect to burned land area, destroyed buildings, and fatalities.

Reviewer: *Further, the manuscript is very short in making reference to previous work. More references to earlier CO work of the MOPITT, SCIAMACHY, IASI, TES, AIRS teams are required.*

Authors: We extended the list of references considerably and give a more comprehensive review of earlier CO work in the revised version.

Reviewer: *What is the scientific value of the paper? The general CO detection capabilities of TROPOMI have been published before [e.g. Borsdorff et al., 2018a,b]. Air quality issues with wild-fire CO emissions are well-known. I would argue that the scientific value is the quantitative estimation of the CO burden (in units mg m^{-3}) based on daily recurrent satellite data i.e. the evaluation of TROPOMI's capabilities for dense CO-related air quality monitoring. Comparison to the CAMS model could also be an added value since it might trigger model improvement. Currently, the methodological evaluation and model comparisons are too short and too vague to serve any of these scientific purposes.*

Authors: We clarified that the main scientific value is indeed the dense daily recurrent satellite monitoring of the CO burden and extended the analysis and discussion of the methodology and the associated uncertainties to serve this interpretation. We also present the comparison to the CAMS model in more detail and discuss differences at a high resolution of $0.1° \times 0.1°$ and the potential of model improvement.

Specific comments

Reviewer: *P4, L11: Please add a discussion on errors coming from the assumptions on boundary layer height knowledge. Discuss how boundary layer height is determined. Please also add figures or tables for typical boundary layer heights. Are boundary layer heights of a few hundred meters (at midday) realistic (P7, L5)? These boundary layer heights need to be validated. If the boundary layer is so shallow, a large fraction of the fire emissions might reach above the boundary layer due to initial thermal rise.*

Authors: We now describe that ERA5 boundary layer heights are defined as the lowest height where the bulk Richardson number, which interrelates stability with vertical wind shear, reaches the critical value of 0.25. We also added a discussion of the uncertainty arising from boundary layer height including the inherent uncertainty estimate based on a 10-member 4D-Var ensemble and the temporal variation of the boundary layer height between 13:00 and 14:00 for a satellite overpass at 13:30 local time. Furthermore, we illustrate the diurnal variations of the boundary layer heights at the analysed cities and fires and compare them to IS4FIRES injection heights to evaluate if the fire emissions might reach above the boundary layer and to determine the uncertainty arising from plume dynamics. It is important to note that the hourly ERA5 boundary layer heights are considerably larger than the boundary layer heights derived in the previous version as the maximum at midday is better sampled due to the better temporal resolution.

Reviewer: *P4, L27: Please add and discuss a figure showing "the fact that the simultaneously retrieved gases, methane and water vapour, are not considerably increased compared to the pre-fire background abundances."*

Authors: In the original manuscript, it could be seen that this is true for the most polluted scene when comparing Figure 6 to Figure 7. In the revised version, we added a figure comprising maps showing the simultaneously retrieved methane abundances for all analysed days. On top of that, deviations of methane from the pre-fire background is also implemented as an alternative quality filter in the revised version because XCH_4 is far less variable than XCO in the presence of wildfires and both gases typically exhibit similar error characteristics (Schneising et al., 2019). Hence, potential issues of the XCO data, for example due to reduced near-surface sensitivity in the presence of clouds or smoke, are clearly detected in the corresponding XCH_4 data and filtered out. The figure also demonstrates that methane is not considerably increased compared to the pre-fire background abundances and that the XCO enhancement patterns are not resembled in XCH_4. Thus, it can be excluded that the detected XCO enhancement is only an artefact as a result of light path lengthening because of aerosol scattering at the particulate matter of the smoke, because such systematic errors would affect both retrieved gases similarly.

Reviewer: *P4, L30: The CAMS comparison is too short to be of scientific value. Please add a quantitative discussion (e.g. average TROPOMI on CAMS resolution and calculate departures).*

Authors: In the revised version, the CAMS near-real-time CO analysis is shown on a finer $0.1° \times 0.1°$ grid and an additional figure is added showing departures to TROPOMI, which is used to discuss the differences in more detail.

Reviewer: *P9, L24: None of the statements in the second paragraph of the conclusion are actually conclusions based on the scientific results of the paper, but rather they are author interpretation of climate change impacts.*

Authors: The revised version includes much more conclusions based on the scientific results of the paper, e.g., concerning TROPOMI's capabilities for dense air quality monitoring on a daily recurrent basis, the potential of model improvement, and the compliance with air quality standards. We highlight that the accurate determination of boundary layer concentrations depends on reliable external mixing layer height information and that the feasibility of the analysis is subject to specific favourable conditions affecting the vertical distribution of emissions in the case of fires to ensure that most of the fire emissions stay within the boundary layer and that pyro-convection or direct injection to the free troposphere is unlikely. Parts of the former second paragraph have been shifted to the introduction or removed.

Reviewer: *Figure 1: This figure could be dropped. The total column sensitivity of the solar absorption concept is standard scientific knowledge. Does the algorithm take into account that the near-ground sensitivity might be reduced due to scattering layers such as wildfire particulate plumes (or low clouds)? If not, what is the impact on the air quality derivations - does the satellite "see" the entire column?*

Authors: The sensitivity depends for example on the spectral resolution and the fitting window used and therefore potentially changes for different instruments or algorithms. Thus, quantitative details of the sensitivity are rather a feature of the instrument and algorithm than of the solar absorption concept. Therefore, it is important to show the averaging kernels. However, as the AKs are now shown in the companion algorithm paper, the figure is dropped here. The newly implemented quality filter based on deviations of simultaneously measured methane from the pre-fire background ensures near-ground sensitivity for all scenes passing the filter. As a consequence, clouds and smoke near the origin of the fires are typically filtered out. However, in sufficient distance of the seat of fire the retrieved abundances are not affected and a quantitative analysis is still possible (e.g., in the analysed major cities), even in cases where efficient scattering in the visible spectral range is indicated by extensive plumes in the VIIRS images. The difference between scattering at clouds and wildfire smoke is the different particle size distribution leading to reduced visibility but far less scattering issues at the smaller particles of smoke in the far field of the fires in the $2.3\,\mu$m spectral range, where the satellite measurements are taken. This is supported by corresponding simulations included in the error analysis to quantify the impact of scattering at smoke aerosols.

Reviewer: *Figures 6 and 7: The figures are too dense with internal information. None of the acronyms (VC, SZA, VZA, dlnI/dx, ...) and few of the terms (sun-normalized radiance) are explained, the panels are too small, some of the panels are not even discussed (Temperature fit, ...). Recommendation: Either remove the figures entirely or just show the relevant parts e.g. the CO panels.*

Authors: Among other things, these figures should have demonstrated that the simultaneously retrieved gases are not considerably increased compared to the pre-fire background abundances, even for the most polluted scenes. As this was not realised by both reviewers, the figures are dropped and the mentioned fact is made more obvious by showing and discussing maps of methane and the newly implemented quality filter.

Anonymous Referee #2

General comments

Reviewer: *The first issue is the lack of any discussion of the retrieval algorithm or the expected error characteristics. References are provided to two ESA technical reports, but these appear not to be peer-reviewed, nor publicly available. A detailed presentation of the retrieval algorithm (in the peer-reviewed literature) is essential for establishing the provenance of the TROPOMI-WFMD CO products. While the general aspects of the algorithm might be similar to published algorithms developed for SCIAMACHY, some details will certainly be instrument-specific. Such details are extremely important.*

Authors: It is true that the two technical reports does not seem to be publicly available and we agree that a detailed presentation of the retrieval algorithm is essential. Therefore, we prepared the companion paper (Schneising et al., 2019) to fulfill this need.

Reviewer: *Similarly, details of the filtering methods (based on CO fit and water vapor absorption) will also influence the scientific interpretation of the data and should therefore also be discussed fully. (For example, how were the thresholds for CO fit and water vapor absorption determined?)*

Authors: The filtering method was updated in the revised version. The standard filter is described and tested in Schneising et al. (2019). It is a machine learning approach trained globally based on cloud data from VIIRS and seems to be rather strict at least for California during the analysed time period, which is indicated by comparison with the VIIRS cloud product for days before the fire. Therefore, a new alternative quality filter for this local application based on deviations of methane from the pre-fire background is implemented and described in the revised version to get a somewhat larger amount of utilisable scenes but retaining good agreement with the VIIRS cloud product. The corresponding methane threshold (3 times the methane random error) was chosen to distinguish systematic from random deviations. As a consequence of the approach, potential issues of the XCO data, for example due to reduced near-surface sensitivity in the presence of clouds or smoke, are clearly detected in the similarly affected XCH_4 data and filtered out.

Reviewer: *The second major area of concern is the lack of any proper validation results; the only mention of validation is a reference to an unpublished technical report. The history of satellite remote sensing demonstrates clearly that satellite products can not simply be taken 'at face value'. For satellite CO products, validation should preferably exploit in-situ CO vertical profiles measured from aircraft. If that approach is not feasible for some reason, the authors could either exploit ground-based FTIR CO retrievals or other satellite CO products. (These latter methods are less optimal than in situ-based methods because of issues related to averaging kernels.) Comparisons of satellite CO products with surface measurements of CO concentration are generally inadequate for validation because of the variability of CO in the middle and upper troposphere.*

Authors: Proper validation with ground-based FTIR retrievals, which are in turn calibrated using in-situ aircraft measurements, is included in the companion paper (Schneising et al., 2019) showing that the TROPOMI/WFMD XCO data set is characterised by a random error (precision) of 5.1 ppb and a systematic error (relative accuracy) of 1.9 ppb. Thereby, averaging kernel issues are appropriately taken into account in the validation as documented in the companion paper.

Reviewer: *Beyond these two major issues, it is not clear how the TROPOMI-WFMD CO product relates to the TROPOMI-SICOR product (as developed by Borsdorff et al.). Do the two algorithms give the same results? Are there other issues which might make one product preferable over the other? Is the TROPOMI-WFMD CO product routinely generated and publicly available? These are inevitable questions that will concern potential users.*

Authors: The companion paper (Schneising et al., 2019) also includes comparisons to the operational product, which uses the SICOR algorithm concluding that both algorithms are highly correlated and show good global agreement although the algorithms differ in several respects. Thus, the scientific and operational products are predestined to be used together with other products in an ensemble approach to benefit from the large range of respective realisations of different physical aspects in the individual retrieval algorithms. This is discussed in the companion paper and is out of the scope of this paper. The TROPOMI/WFMD CO product is routinely generated and publicly available but with time delay.

Reviewer: *My advice to the authors is to strongly consider writing and submitting a validation paper (to AMT or another appropriate journal) which directly addresses these issues. Such a paper is an essential prerequisite to the quantitative use of satellite CO data. Publica-*

tion of that paper would pave the way for this paper and increase its significance.

Authors: The correponding paper addressing the raised issues is available for public review and discussion on AMTD.

Specific comments

Reviewer: *In several places, word choice could be improved to be less sensational and more scientific. For example, in the title, 'Devastating' could be 'Severe'. Similarly, the expression 'burnt to cinders' is gratuitous.*

Authors: We revised the style of the text at several passages and changed the title as suggested.

Reviewer: *p. 2, line 8. Need reference for physiological effects of CO on humans.*

Authors: We added a respective reference (Omaye, 2002).

Reviewer: *p. 2, line 15. The text in this paragraph suggests that MOPITT and IASI CO retrievals are generally insensitive to CO near the surface, but this is overly simplistic. In fact, publications document that both of these instruments can provide useful sensitivity to CO near the surface in daytime scenes over land (i.e., in conditions of high thermal contrast). For example, see "Sensitivity of MOPITT observations to carbon monoxide in the lower troposphere," JGR, 112, doi:10.1029/2007JD008929 (2007) by Deeter et al., and "IASI's sensitivity to near-surface carbon monoxide (CO): Theoretical analyses and retrievals on test cases," JQSRT, 189, doi:10.1016/j.jqsrt.2016.12.022 (2016) by Bauduin et al. MOPITT is also equipped with near-infrared channels which can boost surface-level sensitivity in some scenes.*

Authors: We rephrased the respective passage to avoid this potential misinterpretation and extended the list of references (including, e.g., Deeter et al. (2007), Bauduin et al. (2017), and Worden et al. (2010) for MOPITT's combined TIR/SWIR retrievals) to give a more comprehensive review of earlier CO work.

Reviewer: *p. 4, line 1. If scenes with low clouds are tolerated, what effect does that have on the retrieval vertical sensitivity (averaging kernels)?*

Authors: As already mentioned in the answers to the general comments, the filtering method was replaced in the revised version by a new alternative quality screening algorithn based on deviations of methane from the pre-fire background, which filters out scenes with reduced near-surface sensitivity in the presence of clouds or smoke by detecting significant underestimations in the simultaneously measured XCH_4 data. By construction, all measurements passing this quality filter are sensitive to CO near the surface because both gases, CO and CH_4, typically exhibit similar error characteristics (Schneising et al., 2019).

Reviewer: *p. 4, line 13. The assumption that all of the pyrogenic CO remains in the boundary layer is dubious. Can it be assumed that pyroconvection out of the boundary layer does not occur? After the first day or so of burning, it is likely that CO in the boundary* *layer will start venting into the free troposphere, thus affecting CO concentrations in the free troposphere throughout the region. Finally, there seems to be no consideration of the uncertainty of the boundary layer height.*

Authors: In the revised version, we expanded the analysis, discussion, and conclusions, in particular with respect to the associated uncertainties. We explicitly added an estimation of the uncertainties of the determined concentration anomalies arising from boundary layer height and plume dynamics. The boundary layer heights are also compared to IS4FIRES injection heights to evaluate if the fire emissions might reach above the boundary layer and to determine the uncertainty arising from the vertical distribution of emissions near the source. To this end, we also discuss the local ambient atmospheric conditions (moderate to severe drought), which are favourable for dry smoke plumes being trapped in the boundary layer. We also note that there is no indication for Pyrocumulus or Pyrocumulonimbus in the VIIRS true color images. In summary, it is likely that most of the CO load stays within the boundary layer and that pyro-convection or direct injection to the free troposphere is negligible during the first days of the fire. However, partial venting to the free troposhere cannot be entirely excluded and it is concluded that unknown plume dynamics remains the largest source of uncertainty in the calculation of the boundary layer CO burden caused by wildfires.

Reviewer: *p. 4, line 28. The evidence that light path lengthening (in the presence of smoke) is insignificant is not compelling. The most credible way to prove this claim would involve validation results. If the evidence for this claim is based solely on retrieved amounts of methane and water vapor, those results should be presented in the manuscript to allow the reader to judge whether in fact retrievals of those gases 'are not considerably increased compared to the pre-fire background abundances.'*

Authors: In the original manuscript, it could be seen that the statement is true for the most polluted scene when comparing Figure 6 to Figure 7. In the revised version, we show this more comprehensively by adding a figure showing maps of methane for the analysed days demonstrating that methane is not considerably increased compared to the pre-fire background abundances and that the XCO enhancement patterns are not resembled in XCH4. Thus, it can be excluded that the detected XCO enhancement is only an artefact as a result of light path lengthening because of aerosol scattering at the particulate matter of the smoke, because such systematic errors would affect both retrieved gases similarly. In the error analysis, we also included simulations to quantify the impact of scattering at smoke aerosols.

References

Bauduin, S., Clarisse, L., Theunissen, M., George, M., Hurtmans, D., Clerbaux, C., and Coheur, P.-F.: IASI's sensitivity to near-surface carbon monoxide (CO): Theoretical analyses and retrievals on test cases, J. Quant. Spectrosc. Radiat. Transfer, 189, 428–440, https://doi.org/10.1016/j.jqsrt.2016.12.022, 2017.

Deeter, M. N., Edwards, D. P., Gille, J. C., and Drummond, J. R.: Sensitivity of MOPITT observations to carbon monoxide in the lower troposphere, J. Geophys. Res., 112, https://doi.org/10.1029/2007JD008929, 2007.

Omaye, S. T.: Metabolic modulation of carbon monoxide toxicity, Toxicology, 180, 139–150, https://doi.org/10.1016/S0300-483X(02)00387-6, 2002.

Schneising, O., Buchwitz, M., Reuter, M., Bovensmann, H., Burrows, J. P., Borsdorff, T., Deutscher, N. M., Feist, D. G., Griffith, D. W. T., Hase, F., Hermans, C., Iraci, L. T., Kivi, R., Landgraf, J., Morino, I., Notholt, J., Petri, C., Pollard, D. F., Roche, S., Shiomi, K., Strong, K., Sussmann, R., Velazco, V. A., Warneke, T., and Wunch, D.: A scientific algorithm to simultaneously retrieve carbon monoxide and methane from TROPOMI onboard Sentinel-5 Precursor, Atmos. Meas. Tech. Discuss., https://doi.org/10.5194/amt-2019-243, in review, 2019.

Worden, H. M., Deeter, M. N., Edwards, D. P., Gille, J. C., Drummond, J. R., and Nédélec, P.: Observations of near-surface carbon monoxide from space using MOPITT multispectral retrievals, J. Geophys. Res., 115, D18314, https://doi.org/10.1029/2010JD014242, 2010.

~~Devastating~~ Severe Californian wildfires in November 2018 observed from space: the carbon monoxide perspective

Oliver Schneising, Michael Buchwitz, Maximilian Reuter, Heinrich Bovensmann, and John P. Burrows

Institute of Environmental Physics (IUP), University of Bremen FB1, Bremen, Germany

Correspondence: O. Schneising (oliver.schneising@iup.physik.uni-bremen.de)

Abstract. Due to proceeding climate change, some regions such as California ~~are~~ face rising weather extremes with the dry periods becoming warmer and drier entailing the risk that ~~destructive~~ wildfires and associated air pollution episodes continue to increase. November 2018 has turned into one of the most ~~disastrous months in Californian history~~ severe wildfire episodes on record in California with two particularly destructive wildfires ~~raging~~ spreading concurrently through the North and the South of the state~~leaving about 1000 of land burnt to cinders~~. Both fires ignited at the wildland-urban interface causing ~~at least 88~~ many civilian fatalities and forcing the total evacuation of several cities and communities.

Here we demonstrate that the inherent carbon monoxide (CO) emissions of the wildfires and subsequent transport can be observed from space by analysing radiance measurements of the TROPOspheric Monitoring Instrument (TROPOMI) onboard the Sentinel-5 Precursor satellite in the shortwave infrared spectral range. From the determined CO distribution we assess the corresponding air quality burden in Californian major cities caused by the fires and discuss the associated uncertainties. As a result of the prevailing wind conditions, the largest CO load during the first days of the fires is found in Sacramento and San Francisco with city area averages ~~exceeding boundary layer concentrations of 6~~reaching boundary layer concentration anomalies of about 2.5 ~~and 4 , respectively. For some neighbourhoods in the northwest of Sacramento~~ $\mathrm{mgCO\,m^{-3}}$. Even the most polluted city scenes likely comply with the national ambient air quality standards ($10\,\mathrm{mgCO\,m^{-3}}$ with 8-hour averaging time)~~are likely exceeded.~~. This finding based on dense daily recurrent satellite monitoring is in line with isolated ground-based air quality measurements.

1 Introduction

As a consequence of climate change, precipitation and temperature extremes in California during the cool season (October-May) are occurring more frequently with the dry periods becoming warmer and drier (Swain et al., 2016), which is associated with an increased fire risk. The increasing number of people living in the wildland-urban interface paired with proceeding climate change entailing longer lasting and more intense fire seasons temper the outlook for the future (Radeloff et al., 2018).

The wildfire season 2018 has been the most destructive on record with respect to burned land area, destroyed buildings, and ~~death toll~~ fatalities (California Department of Forestry and Fire Protection, 2018). After a series of ~~blazes~~ conflagrations in July/August including the Mendocino Complex, the largest wildfire in ~~Californian history~~California since the beginning of recording, another round of large wildfires erupted in November, most prominently the Camp Fire and the Woolsey Fire.

The Camp Fire started in the morning of November 8 in Butte County in the North of the state and grew rapidly. It ~~destroyed more than 600 of land, almost 20000 structures, and caused 85 civilian fatalities. As a result, it~~ became both California's most destructive and deadliest wildfire ~~of all time. Several cities and communities had to be evacuated; the town of Paradise was wiped out by the fire.~~

since records began. The Woolsey Fire ignited on the same day as the Camp Fire in the early afternoon near the boundary between Los Angeles and Ventura counties ~~. It~~ and burnt all the way to Malibu~~engulfing about 400 of land, nearly 2000 structures, and killed three people. The fire~~ . Both fires forced the total evacuation of ~~Bell Canyon, Malibu, and Oak Park – an unprecedented instance in history~~several cities and communities.

Smoke from the fires also reached the major cities of the state prompting health warnings and the advice to remain indoors or wear face masks in certain areas (Sacramento Metropolitan Air Quality Management District, 2018; Bay Area Air Quality Management District, 2018). The air quality was affected by particulate matter and carbon monoxide (CO), which results from the incomplete combustion of biomass during wildfires (Yurganov et al., 2005). CO is a colourless, odorless, and tasteless gas that is toxic in large concentrations because it combines with hemoglobin to carboxyhemoglobin, which cannot effectively transport oxygen anymore. ~~It~~ As a consequence, it has the ability to cause severe health problems (Omaye, 2002). CO also plays an important role in tropospheric chemistry being the leading sink of the hydroxyl radical (OH) and acting as a precursor to tropospheric ozone (The Royal Society, 2008).

The Environmental Protection Agency (EPA) is required to set National Ambient Air Quality Standards (NAAQS) for six pollutants considered harmful to public health and the environment, including carbon monoxide, by the Clean Air Act. The CO standards are fixed at $9\,\mathrm{ppm}$ ($10\,\mathrm{mg\,m^{-3}}$) with an 8-hour averaging time, and $35\,\mathrm{ppm}$ ($40\,\mathrm{mg\,m^{-3}}$) with a 1-hour averaging time, neither to be exceeded more than once per year (U.S. Environmental Protection Agency, 2011).

~~Up to now, the satellite-based analysis of CO emissions from fires was typically focused on midtropospheric CO data, e.g., from the Measurement of Pollution in the Troposphere (MOPITT) (Deeter et al., 2018), the~~ Several spaceborne instruments have been measuring CO on a global scale including the Atmospheric Infrared Sounder (AIRS) ~~(Fu et al., 2018),~~ (McMillan et al., 2005), the Tropospheric Emission Spectrometer (TES) (Luo et al., 2015) and the Infrared Atmospheric Sounding Interferometer (IASI) ~~(Turquety et al., 2009) instruments, or~~ (Clerbaux et al., 2009), which observe emissions in the thermal infrared (TIR) and are mainly sensitive to mid/upper-tropospheric ~~CO data from the Microwave Limb Sounder (MLS) (Field et al., 2016)~~ abundances. The sensitivity of TIR satellite sounders to near-surface CO concentrations varies with the thermal contrast conditions (Deeter et al., 2007; Bauduin et al., 2017). The Measurement of Pollution in the Troposphere (MOPITT) instrument (Drummond et al., 2010) combines observations of spectral features in the TIR and in the shortwave infrared (SWIR) to increase surface-level sensitivity in some scenes (Worden et al., 2010). Nearly equal sensitivity to all altitude levels including the boundary layer ~~, where fires are located, was taken advantage of by the Scanning Imaging Absorption Spectrometer for Atmospheric Chartography~~ can be achieved from radiance measurements of reflected solar radiation in the SWIR part of the spectrum. This was first demonstrated by CO retrievals from the SCanning Imaging Absorption spectroMeter for Atmospheric CHartographY (~~(~~SCIAMACHY~~)for cloud-free scenes (Buchwitz et al., 2007; Borsdorff et al., 2018b).~~) instrument (Burrows et al., 1995; B onboard ENVISAT (Buchwitz et al., 2004; de Laat et al., 2010) in the 2.3 µm spectral range.

Up to now, the satellite-based analysis of CO emissions from fires has been utilising profile or column information from, e.g., AIRS (Fu et al., 2018), IASI (Turquety et al., 2009), the Microwave Limb Sounder (MLS) (Field et al., 2016), MOPITT (Deeter et al., 2018), and SCIAMACHY (Buchwitz et al., 2007; Borsdorff et al., 2018b). The recent TROPOMI instrument offers an unique combination of high precision, accuracy, spatiotemporal resolution, boundary layer sensitivity, and global coverage fostering the monitoring of near-ground CO sources (Borsdorff et al., 2018a; Schneising et al., 2019).

2 Data and Methods

In this study, we ~~retrieve and analyse~~ derive and analyse atmospheric carbon monoxide from the radiance measurements of the TROPOspheric Monitoring Instrument (TROPOMI) onboard the Sentinel-5 Precursor (Sentinel-5P) satellite (Veefkind et al., 2012) using the latest version ~~(v1.0)~~ of the Weighting Function Modified DOAS (WFM-DOAS) algorithm ~~(Buchwitz et al., 2006; Schneisin~~ (Buchwitz et al., 2006; Schneising et al., 2011) optimised to retrieve vertical columns of carbon monoxide and methane simultaneously ~~(Schneising, 2017)~~(TROPOMI/WFMD v1.2) (Schneising et al., 2019).

Sentinel-5P was launched in October 2017 into a sun-synchronous orbit with an equator crossing time of ~~1~~13:30 ~~p.m.local time~~. TROPOMI is a spaceborne nadir viewing imaging spectrometer measuring solar radiation reflected by the Earth in a push-broom configuration. It has a swath width of 2600 km on the Earth's surface and covers wavelength bands between the ultraviolet (UV) and the shortwave infrared (SWIR) combining a high spatial resolution with daily global coverage. The horizontal resolution of the TROPOMI nadir measurements, which depends on orbital position and spectral interval, is typically $7 \times 7\,\mathrm{km}^2$ for the SWIR bands used in this study. Due to its wide swath in conjunction with high spatial and temporal resolution, the observations of TROPOMI yield CO amounts and distributions with unprecedented level of detail on a global scale (Borsdorff et al., 2018a). ~~The heritage of the TROPOMI approach to retrieve and comes from the SCIAMACHY project and its observations (Burrows et al., 1995; Bovensmann et al., 1999).~~

As a result of the observation of reflected solar radiation in the SWIR part of the solar spectrum, TROPOMI yields atmospheric carbon monoxide with high sensitivity to all altitude levels including the planetary boundary layer ~~(see Figure ??)~~ and is thus well suited to study emissions from fires. In order to convert the retrieved columns into mole fractions, they are divided by the corresponding dry air column obtained from the European Centre for Medium-Range Weather Forecasts (ECMWF) analysis. The resulting column-averaged dry air mole fractions are denoted by XCO.

~~Column averaging kernels reflecting the altitude sensitivity of the retrievals.~~

Based on a validation with ground-based Fourier Transform Spectrometer (FTS) measurements of the Total Carbon Column Observing Network (TCCON) (Wunch et al., 2011), the TROPOMI/WFMD XCO data set is characterised by a random error (precision) of ~~about 6~~5.1 ppb and a systematic error (relative accuracy) of ~~about 2~~1.9 ppb ~~(Van Roozendael et al., 2018)~~ (Schneising et al., 2019).

~~For the present study a simple~~ The standard quality filter was chosen to be rather strict to meet the demanding requirements on the precision and accuracy of simultaneously retrieved XCH_4 globally. However, a local comparison with the cloud product from the Visible Infrared Imaging Radiometer Suite (VIIRS) instrument (Hutchison and Cracknell, 2005) onboard the joint

NASA/NOAA Suomi National Polar-orbiting Partnership (Suomi-NPP) satellite for days before fire ignition has indicated that the filter can be somewhat relaxed for the present study to maximise the number of utilisable scenes. The implemented alternative quality screening algorithm ~~was implemented excluding measurements not sufficiently characterised by the forward model. It filters out measurements with a~~ is based on simultaneously measured methane and filters scenes where the retrieved $\mathrm{XCH_4}$ is more than 3 times the random error $\approx 50\,\mathrm{ppb}$ smaller than an assumed reference (averaged cloud-free abundances of November 5-7). The threshold was chosen to distinguish systematic from random deviations. Over weakly reflecting ocean or inland water scenes the filter is augmented by additionally flagging scenes with large estimated CO fit error ~~larger than 10% or radiances in specific strong water vapour absorption bands (close to 2.4)larger than 2.5 times the value, which one would expect for cloud-free scenes. For land covered cases, scenes withunrealistically low retrieved surface pressure (difference to ECMWF analysis larger than 300) are also excluded. As a consequence, high clouds are filtered out, while retrievals over low clouds may still be tolerated to some degree, thus increasing the number of utilisable scenes~~($> 10\%$). The rationale behind the use of simultaneously measured $\mathrm{XCH_4}$ as a quality criterion is the following. To begin with, $\mathrm{XCH_4}$ is by far less variable than XCO in the presence of wildfires. Furthermore, both gases typically exhibit similar error characteristics (Schneising et al., 2019). Hence, potential issues of the XCO data, for example due to reduced near-surface sensitivity in the presence of clouds or smoke, are clearly detected in the corresponding $\mathrm{XCH_4}$ data and filtered out.

To get a visual impression of the smoke distribution originating from the fires, so-called true colour images (Red = Band I1, Green = Band M4, Blue = Band M3) from the ~~Visible Infrared Imaging Radiometer Suite (VIIRS) instrument onboard the joint NASA/NOAA Suomi National Polar-orbiting Partnership (Suomi-NPP) satellite~~ VIIRS instrument are used, which show land surface, oceanic and atmospheric features like the human eye would see them (Hillger et al., 2014).

The TROPOMI CO retrievals are also compared to the analysis of the ECMWF Integrated Forecasting System (IFS) provided by the Copernicus Atmosphere Monitoring Service (CAMS) (Inness et al., 2015), which assimilates MOPITT and IASI CO observations ~~(Drummond et al., 2010; Clerbaux et al., 2009)~~ and biomass-burning emissions from ~~MACC's~~ the CAMS Global Fire Assimilation System (GFAS) (Kaiser et al., 2012).

To assess the CO burden in Californian major cities we compute the average total column enhancement (within $20\,\mathrm{km}$ radius around midtown, in units of mass per area) for the first days of the fire relative to November 7, which is considered as background. It is assumed that the additional CO from the fires is located in the well-mixed boundary layer, while the remaining upper part of the contaminated profile closely resembles the background profile, allowing to disentangle the near-surface abundances from the total column measurements. To this end, the total column enhancement is divided by the boundary layer height obtained from the ~~ECMWF analysis~~ hourly ECMWF ERA5 reanalysis product (Hersbach et al., 2018) to get the boundary layer concentration anomaly due to the fires (in units of mass per volume). The ~~areal variation (1σ)~~ ERA5 boundary layer height is defined as the lowest height where the bulk Richardson number, which interrelates stability with vertical wind shear, reaches the critical value of 0.25 (ECMWF, 2018). The associated uncertainty estimates are based on a 10-member 4D-Var ensemble. The areal variation of this anomaly is determined from the standard deviations of the CO columns measuring the inhomogeneity of the boundary layer concentrations within the respective city area. The error analysis includes uncertainties arising from boundary layer height, the vertical distribution of emissions near the source, and

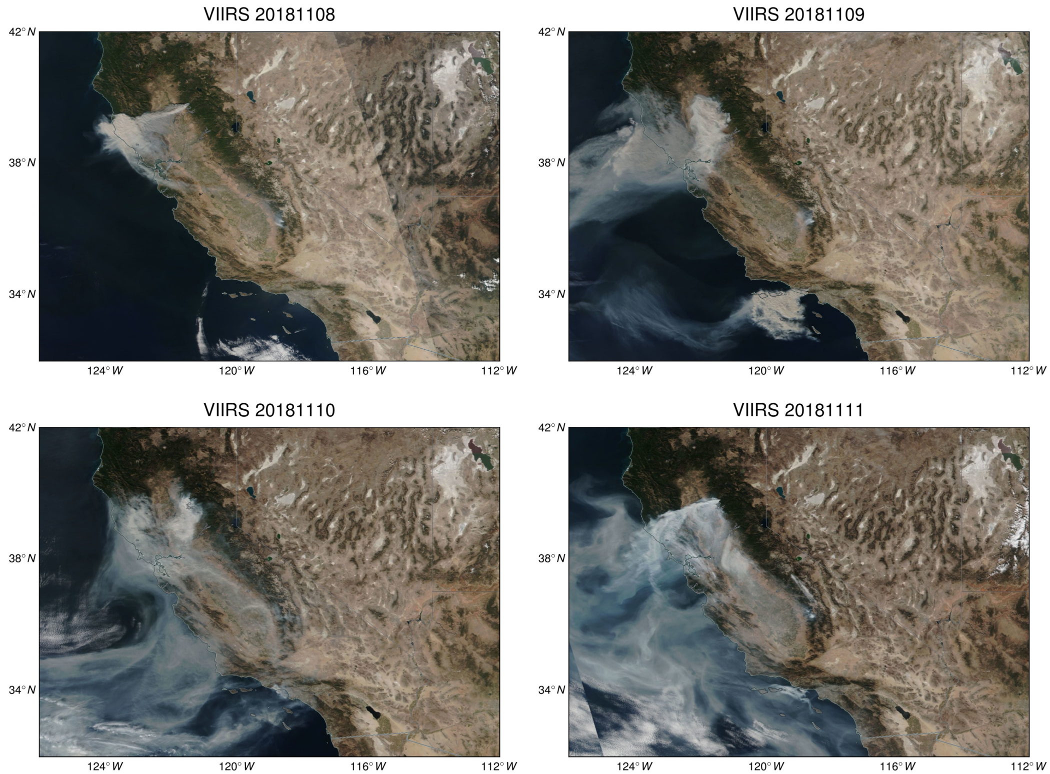

Figure 1. True colour reflectances from the Visible Infrared Imaging Radiometer Suite (VIIRS) for the first days of the fires taken from the NASA Worldview application.

smoke aerosol. Thereby, gridded Integrated Monitoring and Modelling System for wildland fires (IS4FIRES) injection heights (Sofiev et al., 2012) (corresponding to the top of the plume) as obtained from the CAMS GFAS are used to estimate how much of the pyrogenic CO may leave the boundary layer.

3 ~~Results~~

3 Results and Discussion

3.1 Quality filtered XCO and comparison to CAMS

As a result of the Camp and Woolsey fires ignited on November 8, associated smoke overcast large parts of the state for days. This can clearly be seen on the VIIRS true colour images in Figure 1. Sentinel-5 Precursor and Suomi-NPP fly in loose formation, with Sentinel-5P trailing behind by 3.5 minutes, ensuring that both satellites observe (almost) the same scene. Thus, the corresponding images can be compared directly. ~~Figure~~

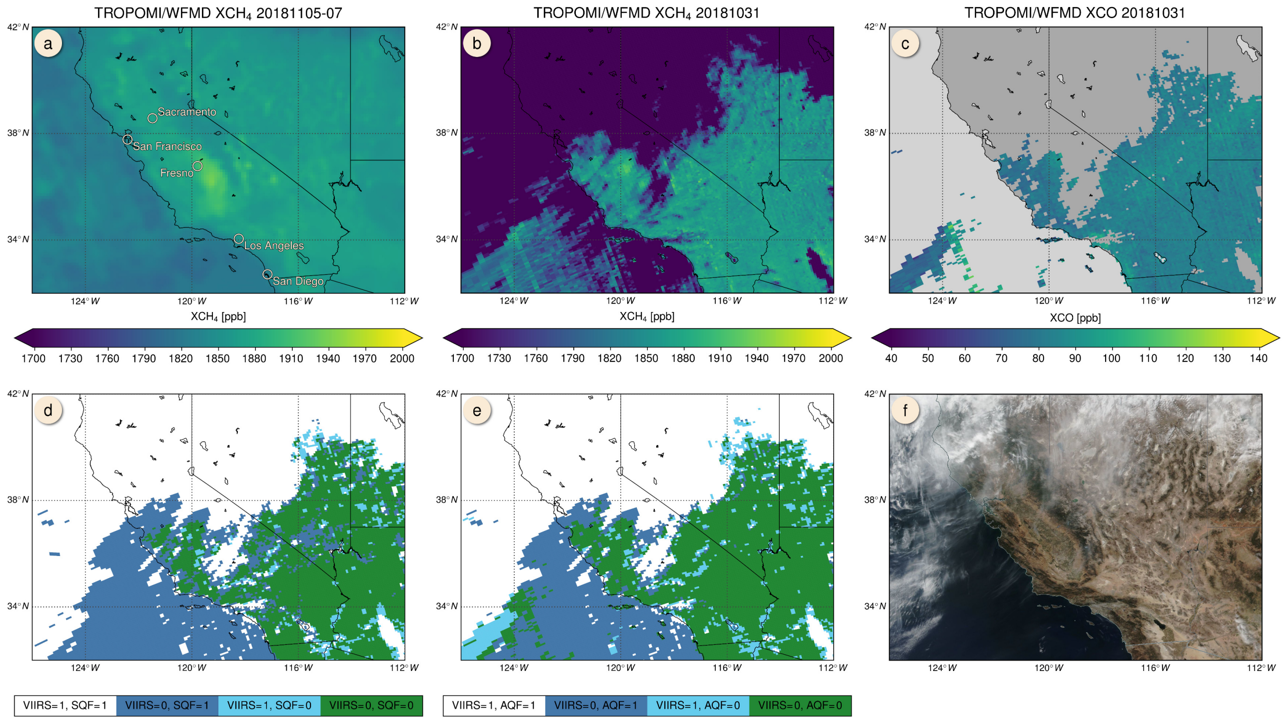

Figure 2. Performance of the implemented quality filter for the example day October 31. a) Cloud-free reference XCH_4 abundances (November 5-7). b) Unfiltered XCH_4 data. c) XCO after application of the filter removing scenes with unrealistic low XCH_4. d) Comparison of the standard quality filter (SQF) with the VIIRS cloud classification (1=filtered out). Matching classifications are shown in white and green (agreement with VIIRS: 78%, passing SQF: 32%). e) As before but for the alternative quality filter (AQF) used in the presented analysis (agreement with VIIRS: 81%, passing AQF: 39%). f) VIIRS true color image.

The performance of the quality filter based on simultaneously measured methane is demonstrated in Figure 2 for an example day before the start of the analysed fires. In line with the error analysis based on synthetic data presented in Schneising et al. (2019) , there typically is a considerable underestimation of XCH_4 in the presence of clouds due to shielding of the underlying partial columns. After application of the alternative quality filter, there are no obvious issues with the XCO data. The relaxed quality screening algorithm provides similar results to the standard filter concerning the overall agreement rate with the VIIRS cloud product, but actually yields more scenes passing the filter (about 20% for the analysed example day).

Figure 3 shows the daily XCH_4 distribution over California, which is used for quality screening. For each day, XCH_4 resembles the pre-fire background abundances shown in Figure 2a with the exception of considerable underestimations here and there mainly due to reduced near-surface sensitivity in the presence of clouds or smoke near the origin of the fires. However, in sufficient distance of the seat of fire the XCH_4 abundances are not affected and a quantitative analysis is still possible, even in cases where efficient scattering in the visible spectral range is indicated by extensive plumes in the VIIRS images. The explanation for this is the particle size distribution of the wildfire smoke. While clouds typically consist of water droplets

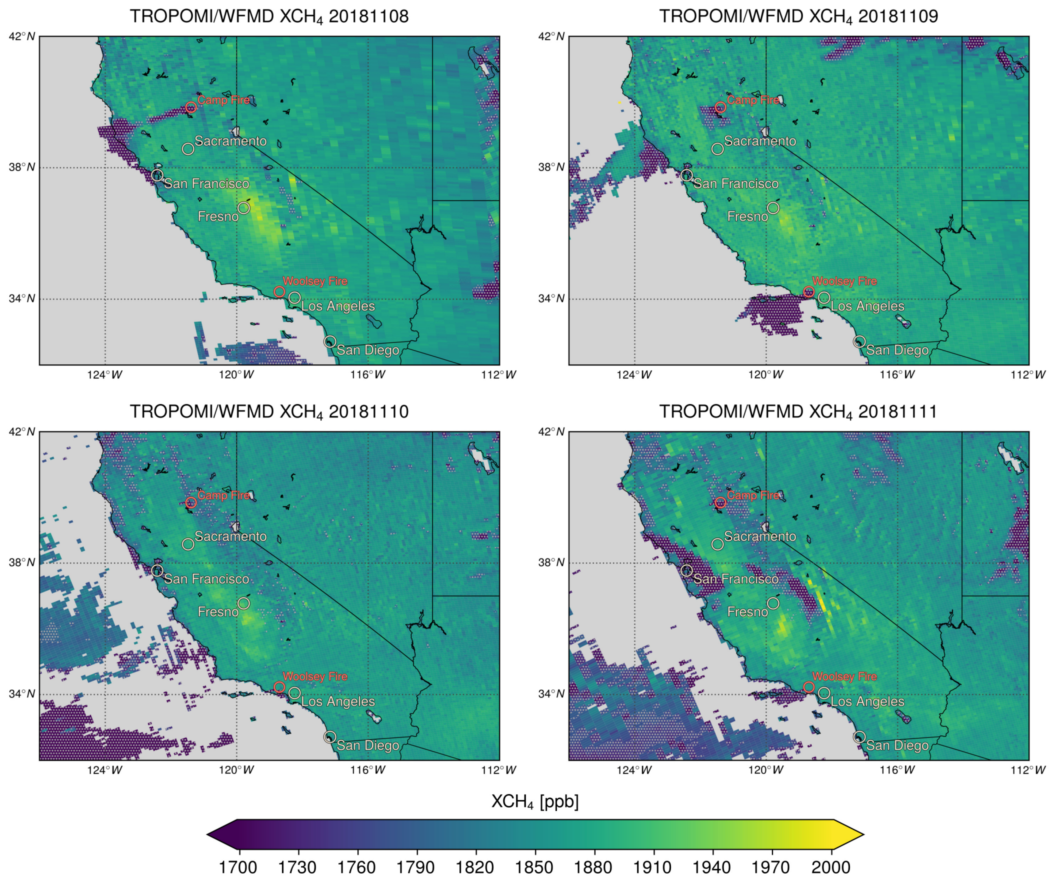

Figure 3. Retrieved methane column-averaged mole fractions from TROPOMI for the same days as in Figure 1. The $\mathrm{XCH_4}$ is used to filter out scenes with significant underestimation (dotted scenes) mainly due to reduced near-surface sensitivity in the presence of clouds or smoke due to shielding of the subjacent partial columns. The Central Valley exhibits combined anthropogenic methane emissions from oil fields and agriculture (Schneising et al., 2019).

with an effective radius of the order of 10 µm, smoke is dominated by considerably smaller particles. The mass distribution of smoke plumes shows a prominent peak at about 0.3 µm (Stith et al., 1981) but is nevertheless dominated by a small number of supermicron-sized particles including some very large particles (Radke et al., 1990). As a consequence of the different size distributions, clouds have a typical Ångström exponent $\alpha = 0$ and thus no wavelength dependence of the aerosol optical depth, while biomass burning aerosols have a distinct wavelength dependence with typical α ranging between 1 and 2 depending on the fire (Eck et al., 2009). The submicron particles reduce the visibility and lead to extended smoke plumes over large distances in the VIIRS true color reflectances shown in Figure 1. However, the 2.3 µm spectral range, where the satellite measurements are taken, is subject to only little scattering at these small particles. The satellite retrievals close to the source of the fire are rather affected by the large supermicron-sized particles, which have a short atmospheric lifetime tending to fall out rapidly

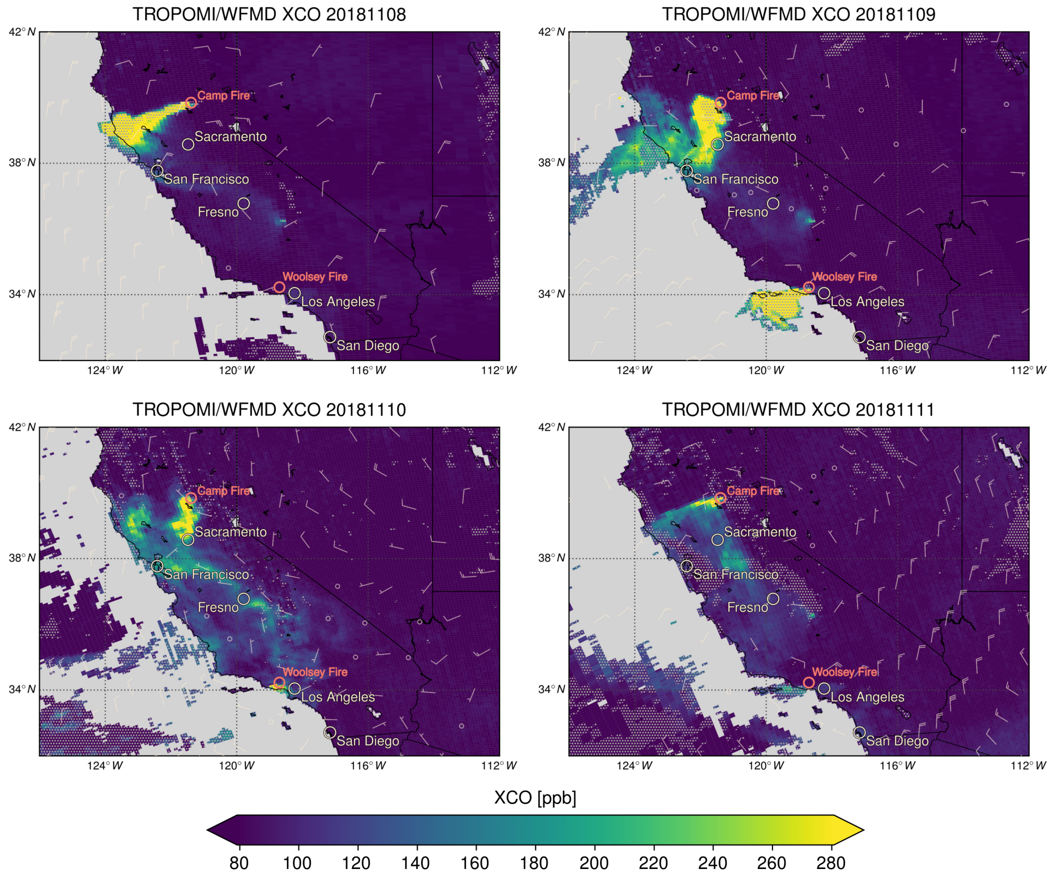

Figure 4. Retrieved carbon monoxide column-averaged mole fractions from TROPOMI for the same days as in Figure 1. Dotted scenes are excluded by the quality filter based on simultaneously retrieved XCH_4. Also shown is the mean wind in the boundary layer obtained from ECMWF data.

(World Health Organization, 2006) and are thus getting more and more negligible when departing from the seat of fire. Thus, a reliable XCO retrieval is possible in smoke plumes in the far field of the fire origin for scenes passing the quality filter. Corresponding simulations with realistic aerosol optical depth and Ångström exponent are included in the error analysis in the next subsection to quantify the impact of scattering at smoke aerosols.

Figure 4 shows the XCO distribution over California, which obviously matches the smoke emission and transport patterns detected by VIIRS unambiguously. This substantiates that the observed CO enhancements are actually originating from the wildfires. It can be seen that the abundances over the major cities we want to analyse are typically not filtered out and are thus suitable for a quantitative analysis. However, the quantitative interpretation of scenes right above or too close to the origin of the fire is limited by reduced vertical retrieval sensitivity near the surface and are consequently filtered out.

~~True colour reflectances from the Visible Infrared Imaging Radiometer Suite (VIIRS) for the first days of the fires taken from the NASA Worldview application.~~

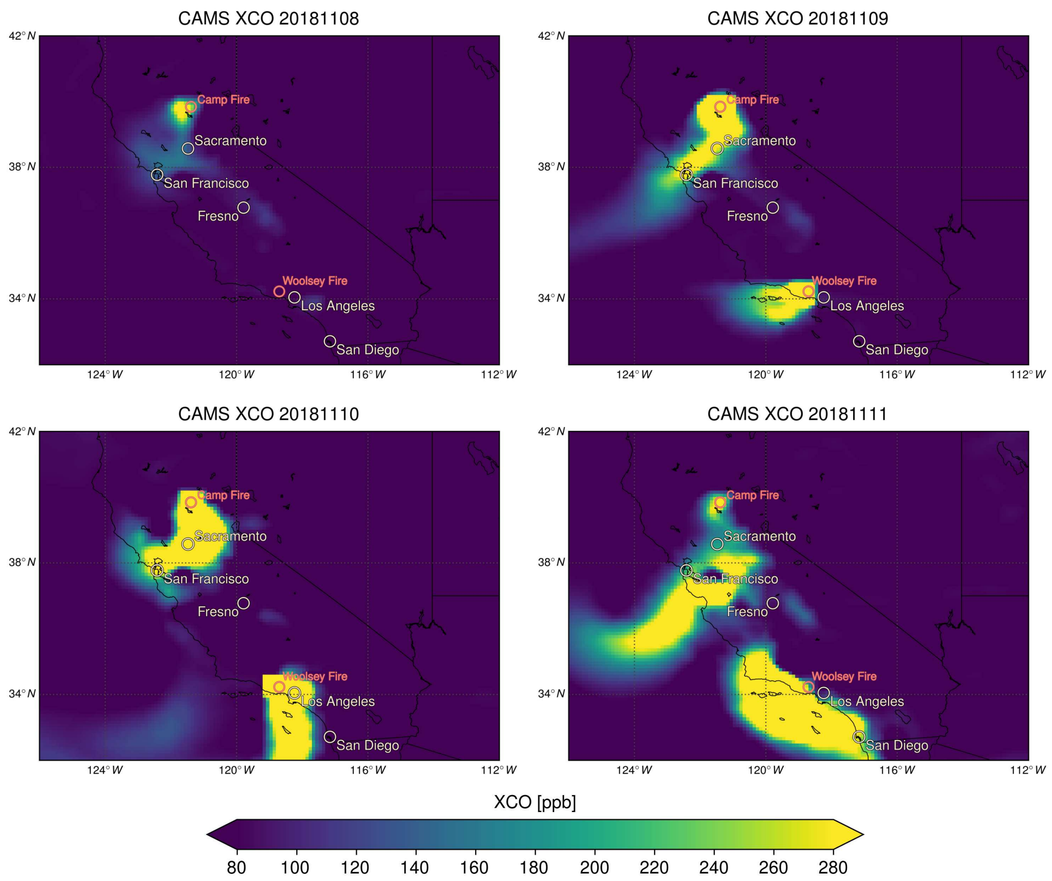

Figure 5. CAMS near-real time CO analysis for the first days of the fires at 24:00 UTC corresponding to 16:00 local time (Pacific Standard Time).

~~Retrieved carbon monoxide column-averaged mole fractions from TROPOMI for the same days as in Figure 1. Also shown is the mean wind in the boundary layer obtained from ECMWF data.~~

~~It is important to note that it can be excluded that the satellite-derived statewide column enhancement is only an artefact as a result of light path lengthening because of aerosol scattering at the particulate matter of the smoke. This is verified by the fact that the simultaneously retrieved gases, methane and water vapour, are not considerably increased compared to the pre-fire background abundances; light path related systematic errors would affect all retrieved gases similarly.~~

For comparison, Figure 5 shows the CAMS near-real-time CO analysis on a ~~$0.75° \times 0.75°$~~ $0.1° \times 0.1°$ grid for the same days shown in the previous figures ~~close to the time of~~ and the closest available time to the TROPOMI overpass ~~.~~ at 13:30 local time. As CAMS is available in time steps of 6 hours, the analysis corresponding to 16:00 local time is used for the comparison. Although CO emissions from the fires are obviously included in the CAMS data, the transport patterns ~~and intensity distribution~~ seem to be somewhat different~~, e. g., abundances on November~~ . While the patterns are broadly consistent for November 9 and 10, the modelled wind fields close to the fires seems to deviate on November 8 and 11~~are predicted to be considerably larger than measured by the satellite, whereas they are predicted to be considerably smaller on November 8.~~ , which results in a longer continuance of the plume over land, while the VIIRS images and the TROPOMI data suggest a faster transport westwards to the sea. This can also be seen in Figure 6 showing departures of the CAMS analysis from the TROPOMI XCO after averaging the satellite data on the CAMS resolution. Apart from the partially different transport patterns, also the intensity distribution close to the fire sources is different, with CAMS abundances being considerably higher for the most part and deviations reaching several hundred ppb. This may be due to overestimated wildfire fluxes, underestimated initial horizontal transport in the vicinity of the fire sources, or a combination of both.

3.2 Boundary layer concentration anomalies and associated uncertainties

To assess the CO ~~analysis for~~ burden in Californian cities, the boundary layer CO concentration anomaly $\Delta\rho_{bl}$ is computed in the following way from the total column enhancement Δv_{CO} (in units of molecules per area) relative to the pre-fire background

$$\Delta\rho_{bl} = \frac{\Delta v_{\mathrm{CO}} \cdot M_{\mathrm{CO}}}{N_A \cdot A \cdot h_{bl}} \tag{1}$$

where $M_{\mathrm{CO}} = 28\,\mathrm{g\,mol^{-1}}$ is the molar mass of carbon monoxide, $N_A = 6.022 \cdot 10^{23}\,\mathrm{molec\,mol^{-1}}$ is the Avogadro constant, $A = 0.95$ is the dimensionless near-surface averaging kernel of the retrieval for appropriate conditions, and h_{bl} is the height of the boundary layer, in which pollutants are fully mixed vertically. The boundary layer height detemines the available volume for pollution dispersion and is thus a critical parameter for air quality assessment.

The diurnal variation of the ECMWF ERA5 boundary layer heights and their inherent uncertainties are illustrated in Figure 7. There is a strong diurnal cycle with low values at night and maximal values around local noon close to the time of the TROPOMI overpass at 13:30. The boundary layer concentration uncertainty arising from boundary layer height $\sigma(h_{bl})$ is determined from the maximal ERA5 ensemble uncertainty between 13:00 and 14:00 local time and the variation within this hour in each case. Typical values of $\sigma(h_{bl})$ range between 10% and 25%.

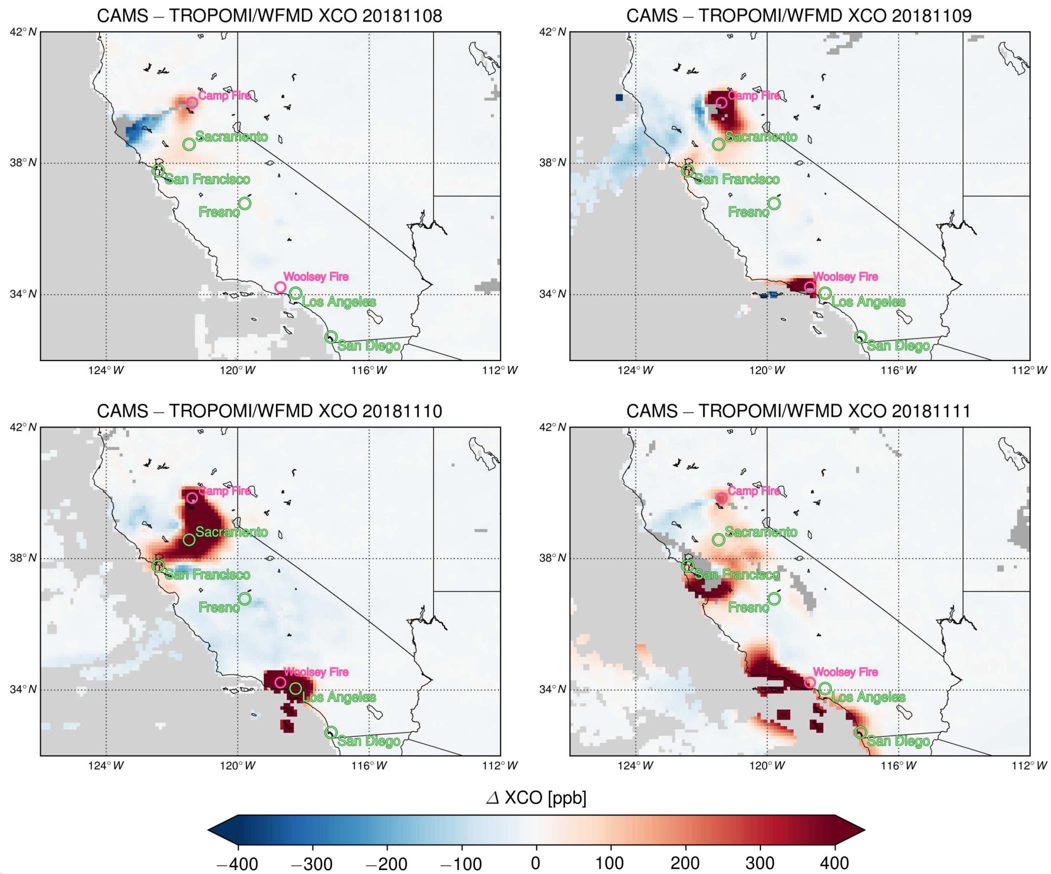

~~CAMS near-real time~~

Figure 6. Difference of CAMS XCO analysis to TROPOMI/WFMD satellite measurements.

The potentially largest source of uncertainty in calculation of the boundary layer CO burden is plume dynamics and the question if all CO remains in the boundary layer or if a certain proportion reaches the free troposphere. The vertical distribution of emissions near the source is driven by the fire radiative power and the local ambient atmospheric conditions such as stability and humidity. Three types of wildfire plumes are distinguished by the amount of condensed water vapour during plume formation (Fromm et al., 2010): 1) Dry smoke plumes, which contain water vapour and usually stay within the boundary layer, 2) Pyrocumulus containing water droplets either staying in the boundary layer or reaching the free troposphere depending on atmospheric conditions, and extreme 3) Pyrocumulonimbus scenarios containing ice particles and potentially reaching the stratosphere. Typically, most of the biomass burning emissions stay within the mixing layer and cases with pyro-convection or direct injection to the free troposphere or even higher are rare (Labonne et al., 2007; Mazzoni et al., 2007; Tosca et al., 2011).

As can be seen in Figure 7, the IS4FIRES injection heights corresponding to the top of the plume are equal or smaller than the respective maximum boundary layer height at the location of the fires, with the exception of the first day of the Camp Fire. This sole discrepancy may be linked to overestimated fire radiative power for the Camp Fire on the day of ignition, which is also

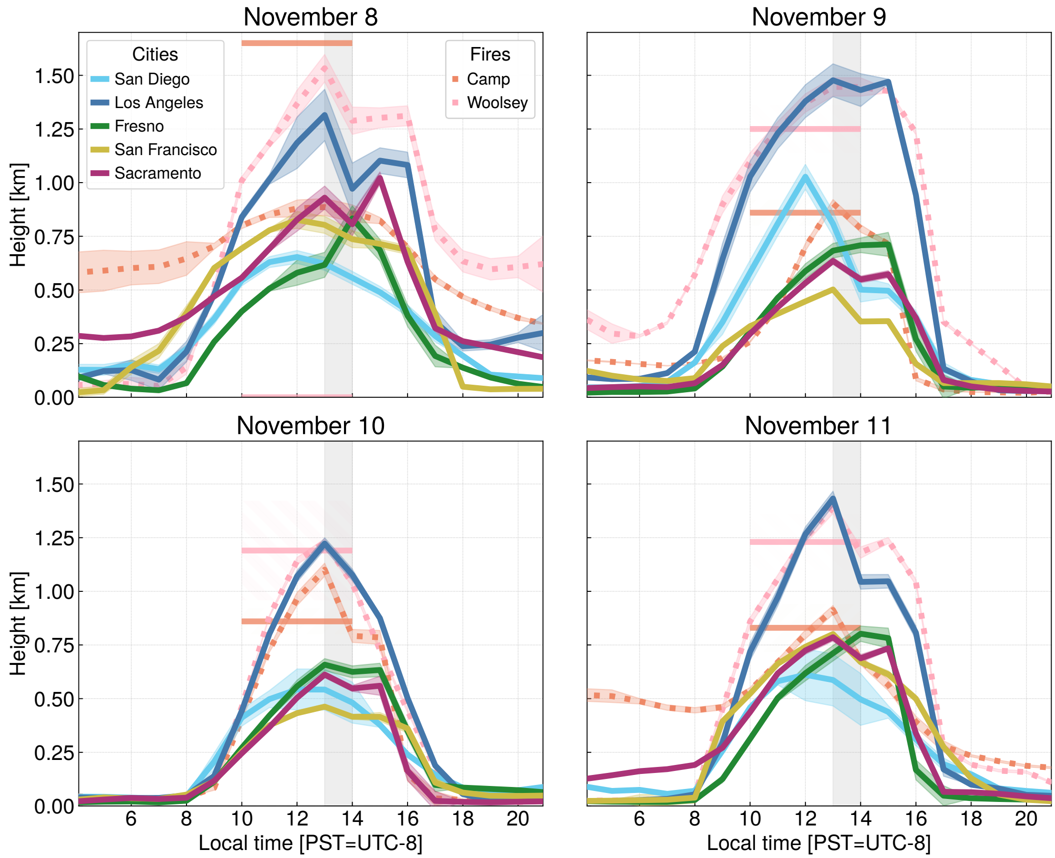

Figure 7. Diurnal variations of the boundary layer heights obtained from the ECMWF ERA5 reanalysis for major Californian cities (solid) and fires (dotted). The uncertainty estimates are based on a 10-member 4D-Var ensemble. Also shown are mean IS4FIRES smoke injection heights and their variation for both analysed fires as horizontal bars and surrounded hatched areas. The grey-shaded area illustrates the TROPOMI overpass time. On November 8 the injection height of the Woolsey Fire is zero because it started later in the day.

suggested by the comparison of the CAMS XCO analysis to the TROPOMI retrievals showing considerably higher abundances for CAMS in the vicinity of the fire source. In summary, the IS4FIRES injection height analysis indicates that most of the CO load stays within the boundary layer. Furthermore, entire California was at least abnormally dry within the analysed time period with a moderate drought at the Camp Fire origin and a severe drought at the seat of the Woolsey Fire according to the United States Drought Monitor (https://droughtmonitor.unl.edu/). These are favourable conditions for dry smoke plumes being trapped in the boundary layer also rendering later deep moist convection with transport to the free troposphere at another time and location unlikely. Finally, there is also no indication for Pyrocumulus or Pyrocumulonimbus in the VIIRS true color images. Nevertheless, partial venting to the free troposhere cannot be entirely excluded and we therefore introduce a generic uncertainty $\sigma(h_{inj})$ of 25% arising from unknown plume dynamics, which is only applied to the smaller end of the boundary layer concentration anomaly because lost CO of this type can only lead to an overestimation of the near-surface concentrations.

Another potential error source associated with fires is smoke aerosol. Scenes with reduced near-surface sensitivity due to clouds and smoke with large particles near the seat of the fires are automatically filtered out using simultaneously measured methane. Figure 3 also demonstrates that methane is not considerably increased compared to the pre-fire background abundances (Figure 2a) and that the XCO enhancement patterns are not resembled in XCH_4. Thus, it can be excluded that the detected XCO enhancement is only an artefact as a result of light path lengthening because of aerosol scattering at the particulate matter of the smoke, because such systematic errors would affect both retrieved gases similarly.

To assess the potential impact of smoke aerosol quantitatively, simulated measurements are used. This means that radiances and irradiances for an assumed smoke scenario are calculated with the radiative transfer model, which are subsequently used as measurement input in the retrieval. The errors are then defined as the deviation of the retrieved columns for the smoke scenario from the corresponding columns for the background scenario also used to calculate the forward model look-up table. To model wildfire conditions in sufficient distance from the seat of the fire with low visibility but decreasing scattering issues at larger wavelengths (consistent with Figures 1 and 3) we use the *extreme in BL* aerosol scenario originally introduced in Schneising et al. (2008) containing urban aerosol with a significant soot fraction (Shettle and Fenn, 1979) combined with an extreme CO profile with an 10-fold enhancement in the boundary layer compared to the standard profile. The used aerosol scenario (aerosol optical depth $\tau_{550\,\mathrm{nm}} \approx 3$ and Ångström exponent $\alpha \approx 1$) is considered a realistic worst case scenario because it is at the upper end of optical depths and at the lower end of Ångström exponents for typical fire aerosols (Eck et al., 2009) . Thus, most fires exhibit less scattering in the 2.3 µm spectral range than our model scenario assumes. The corresponding results are summarised in Figure 8. Typical systematic CO errors for Californian cities on the analysed days range between about -3% and 2% for the assumed aerosol type and CO profile. Therefore, the uncertainty due to smoke aerosol $\sigma(a_{smo})$ is set to 5% adding an extra amount due to the uncertainty of the actual aerosol type.

The total uncertainty of the boundary layer concentration anomaly $\sigma(\Delta\rho_{bl})$ is determined by

$$\sigma^2(\Delta\rho_{bl}) = \sigma^2(h_{bl}) + \sigma^2(h_{inj}) + \sigma^2(a_{smo}) \qquad (2)$$

Averaged boundary layer concentration anomalies of CO (relative to November 7) in major Californian cities during the first days of the Camp and Woolsey fires are presented in ~~Table ??~~Figure 9 together with the total uncertainty of Equation 2 and an estimate of the areal variation measuring the inhomogeneity of the CO concentrations within the city area. The largest values ~~were~~ are found for Sacramento and San Francisco on November 9 and 10 ~~,~~ due to the prevailing wind conditions ~~, exceeding concentrations of 6~~with boundary layer concentration anomalies of about 2.5 ~~and 4, respectively, which is about half of~~ $\mathrm{mgCO\,m^{-3}}$, which is well below the national CO air quality standard of $10\,\mathrm{mg\,m^{-3}}$ even after adding a typical background concentration of about 0.5–1.0 $\mathrm{mgCO\,m^{-3}}$. The cities in the ~~South~~ southern part of the state are less affected owed to more ~~favorable~~ favourable weather conditions.

Although the Sacramento and San Francisco city averages are compliant with air quality standards, the large associated areal variations indicate an uneven CO distribution within both towns, in particular for Sacramento. This interpretation is supported

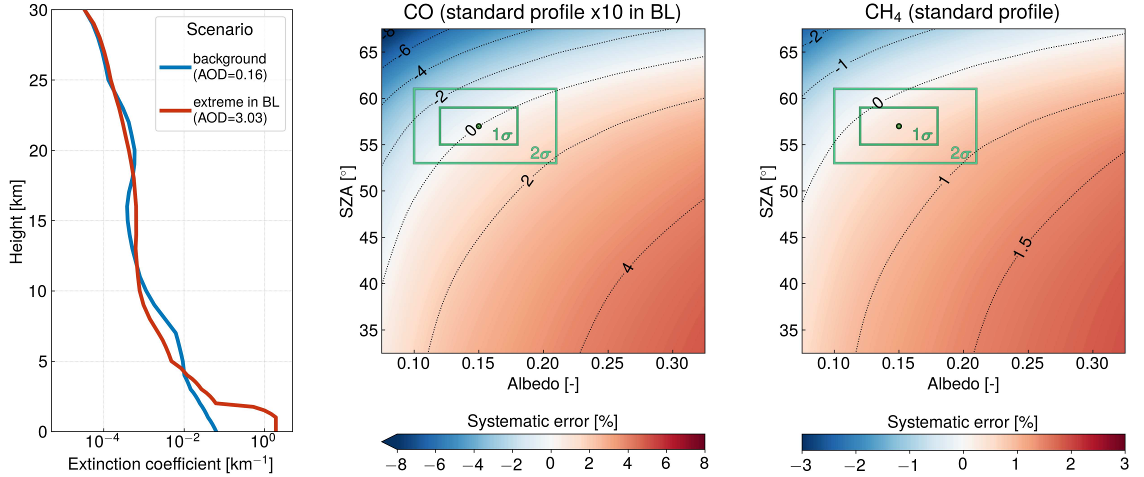

Figure 8. The left panel shows the ~~first days~~ aerosol extinction profiles used in the analysis of smoke aerosol errors. Also given are the ~~fires~~ corresponding aerosol optical depths at ~~9 p.m. UTC (Coordinated Universal Time)~~ 550 nm. The other panels show the systematic errors of CO and CH_4 as function of solar zenith angle and albedo when using the extreme instead of the background aerosol scenario. The green boxes highlight the typical conditions for the Californian cities on the analysed days using percentiles corresponding to ~~1 p.m. local time~~ 1σ (~~Pacific Standard Time~~68% of data) and 2σ (95% of data). The green circle is the pair of median albedo and median solar zenith angle.

by the CO distribution depicted in Figure 4 showing that the plume's edge of the Camp Fire is located near Sacramento leading to a larger burden in the northwest compared to the rest of the city.

The largest ~~total column value~~ burden with respect to CO within all city radii is actually found on November 10 ~~near~~ about 10 km to the east of Sacramento International Airport~~. The corresponding spectral fit is shown in Figure ?? demonstrating a massive load and that the fit residual is small relative to the individual scaled derivatives (weighting functions) with respect to all fit parameters including the weak absorption. When compared to a nearby background scene from November 7 (see Figure ??),~~ , where one finds a considerable column enhancement of ~~3.0~~3.14 $\mathrm{g\,m^{-2}}$. Given the ECMWF ~~analysis~~ ERA5 boundary layer height of ~~171~~580 m, this corresponds to a boundary layer concentration anomaly of ~~17.5~~5.42 $\mathrm{mgCO\,m^{-3}}$ ~~. The corresponding~~ [3.97–5.96; 1σ]. The largest enhancement on November 9 ~~at the same location was 2.1~~is also located in the vicinity of Sacramento Airport (about 10 km to the southwest) and amounts to 3.13 $\mathrm{g\,m^{-2}}$ with a boundary layer height of ~~266~~592 m leading to a boundary layer concentration anomaly of ~~7.9~~5.28 $\mathrm{mgCO\,m^{-3}}$ [3.83–5.89; 1σ]. Thus, ~~it is reasonable to assume that~~ the national ambient air quality standard of 10 $\mathrm{mgCO\,m^{-3}}$ was likely ~~exceeded for at least one 8-hour average in some neighbourhoods in the northwest of Sacramento~~not exceeded even for the most polluted city scenes and after adding a typical background of about 0.5–1.0 $\mathrm{mgCO\,m^{-3}}$.

~~Example spectral fit for a contaminated scene (white circle on the map) on November 10 near Sacramento International Airport. The different colours on the map represent different surface types (United States Geological Survey, 2018). On the left, the measured sun-normalised radiance (red), the fitted WFM-DOAS linearised radiative transfer model (black), and the~~

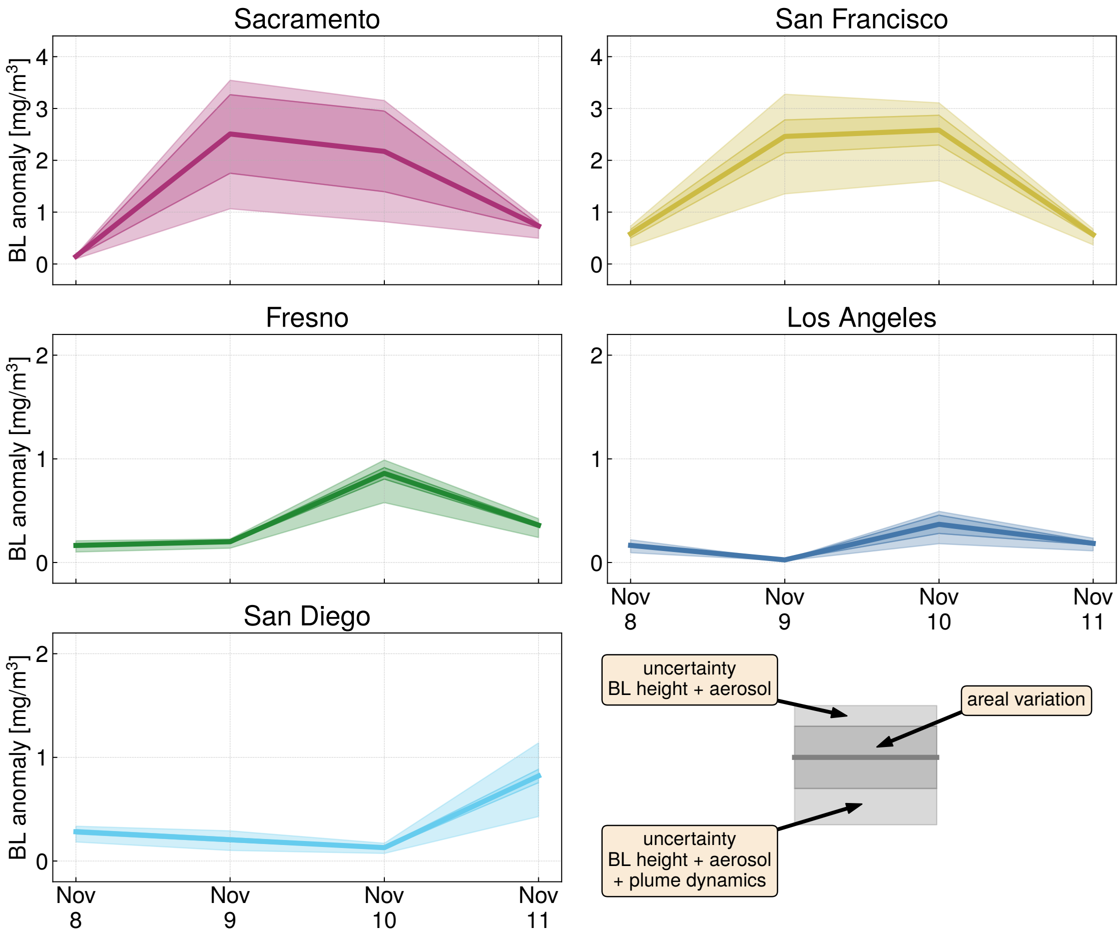

Figure 9. Averaged boundary layer concentration ~~anomaly~~ anomalies of CO (relative to November 7) and associated areal ~~variation~~ variations and uncertainties (1σ) in major Californian cities during the first days of the Camp and Woolsey fires.

~~November 8 November 9 November 10 November 11 Sacramento 0.21 ± 0.04 4.80 ± 2.25 6.64 ± 3.93 1.43 ± 0.15 San Francisco 0.67 ± 0.23 4.14 ± 0.86 3.99 ± 0.94 0.57 ± 0.19 Fresno 0.26 ± 0.05 0.60 ± 0.15 2.02 ± 0.28 1.10 ± 0.20 Los Angeles 0.32 ± 0.05 0.15 ± 0.09 1.43 ± 0.89 0.43 ± 0.09 San Diego 0.42 ± 0.07 0.25 ± 0.09 0.23 ± 0.09 0.99 ± 0.13~~

~~resulting fit residual are shown. The right-hand panels compare the sum (red) of scaled derivative and fit residual to the scaled derivative itself (black) for each fit parameter. The fit residual is considered small because the red symbols follow the spectral features of the respective black line.~~

~~Background scene on November 7 for the contaminated scene near Sacramento International Airport shown in Figure ??.~~

To further assess the described area with significantly increased boundary layer concentrations, we revisit the discussed contaminated scene near Sacramento International Airport on November 10 and analyse associated results from CAMS and ground-based Quality Assurance Air Monitoring Site Information. For the grid-box comprising the mentioned satellite scene, CAMS predicts ~~an even~~ a considerably larger column enhancement of ~~7.0~~5.93 $\mathrm{g\,m^{-2}}$ corresponding to a boundary layer concentration anomaly of ~~34.4~~10.23 $\mathrm{mgCO\,m^{-3}}$~~(boundary layer height of 202 according to the ECMWF analysis). However, the scene is located near the bottom edge of the rather large CAMS grid-box expanding further north in the direction of the fire origin. This potentially explains the large boundary layer concentration~~, which is almost twice as high as the satellite derived concentration anomaly and potentially exceeds the national ambient air quality standards.

Ground-based measurements are available from the Air Quality and Meteorological Information System (AQMIS) network (California Air Resources Board, 2018) ~~. Unfortunately, there are only two~~ providing daily maximum and daily average values. There are three CO measurement sites in Sacramento County~~and~~. However, the analysed data for November 2018 has to be considered preliminary according to the network operators. For the site at Bercut Drive in Sacramento ~~most of the data is missing~~ the data set is incomplete during the first days of the fire and therefore excluded from the comparison. The second site at Blackfoot Way in North Highlands is located farther north and closer to the analysed contaminated satellite scene. ~~This site also exhibits large data gaps for the analysed time period. On November 10, 50% of the hourly data are missing reducing the significance of the daily maximum 1-hour average value, which~~ The maximum value during the first four days of the fire is stated to be ~~4~~4.1 ppm (~~4.6~~4.7 $\mathrm{mgCO\,m^{-3}}$) ~~.~~on November 10. Relative to the maximum value of November 7 this corresponds to a concentration anomaly of 3.53 $\mathrm{mgCO\,m^{-3}}$. The third site is at Del Paso Manor in Sacramento with an maximum value of 3.8 ppm (4.3 $\mathrm{mgCO\,m^{-3}}$) on November 10 corresponding to a concentration anomaly of 2.95 $\mathrm{mgCO\,m^{-3}}$. When using the daily averages instead of the maximum values, the concentration anomalies amount to 1.89 $\mathrm{mgCO\,m^{-3}}$ for both sites.

Figure 10 shows the boundary layer concentration anomalies of Sacramento and its surrounding districts allowing to get an overview of the situation by highlighting the locations of the different measurements. As can be seen, the AQMIS ~~site is~~ sites are located easterly of the satellite scene with maximal city area CO value, where concentrations are beginning to decline steeply. The corresponding satellite ~~average for the North Highlands site is estimated to be 6.28 ± 2.72, which is broadly consistent with the maximal daily~~ averages at both analysed AQMIS sites are broadly consistent with the ground-based measurements taking into account the potential variability within a satellite scene indicated by the scene-to-scene gradient of the satellite data and the fact that the sites are located at the edge of satellite scenes. While the ground-based anomaly based on the maximum values in North Highlands matches well with the value of the associated satellite scene, the ground-based ~~measurements.~~ anomaly based on the daily averages rather resembles the values of adjacent satellite scenes to the east or to the south. At Del Paso Manor it is the other way round: the ground-based anomaly based on the daily averages fits the surrounding satellite scene well, while the anomaly based on the maximum values rather matches the adjacent satellite scene to the north.

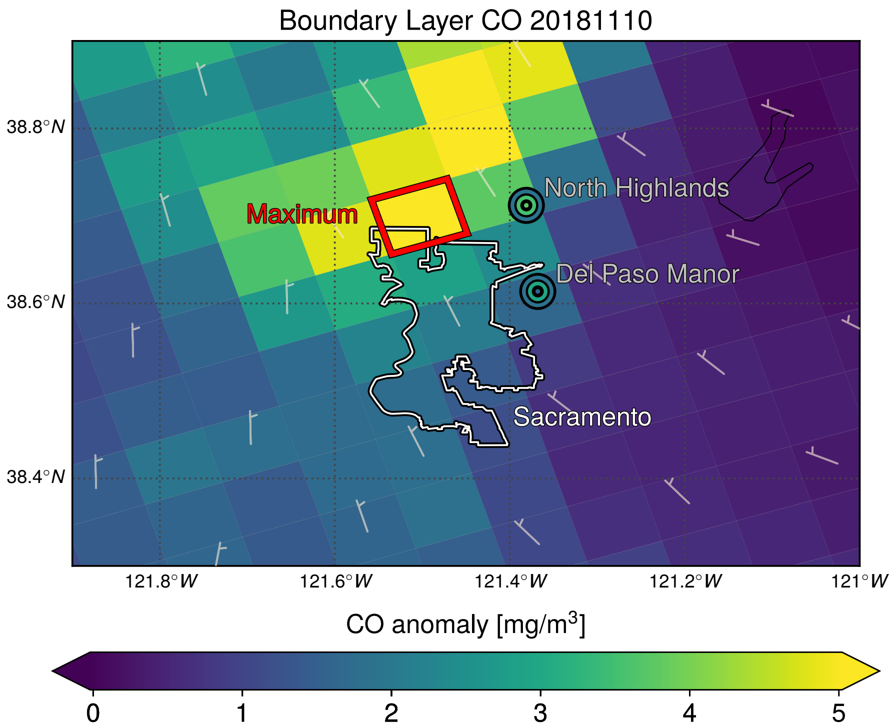

Figure 10. Boundary layer concentration anomalies of Sacramento and its environs determined from TROPOMI CO total column measurements and boundary layer heights from the ECMWF ERA5 reanalysis. Highlighted are the satellite scene with maximal city area value (5.42 $\mathrm{mgCO\,m^{-3}}$ [3.97–5.96; 1σ], red) and the location of the AQMIS sites in North Highlands and at Del Paso Manor (black). The anomalies based on the maximum values of the ground-based sites (3.53 and 2.95 $\mathrm{mgCO\,m^{-3}}$) are colour-coded in the inner circle at the site location, the anomalies based on the daily averages (1.89 $\mathrm{mgCO\,m^{-3}}$ each) are colour-coded in the outer circle.

~~Boundary layer concentration anomalies of Sacramento and its environs determined from TROPOMI CO total column measurements and boundary layer heights from the ECMWF analysis. Highlighted are the satellite scene with maximal city area value (17.5 , red) and the location of the AQMIS site in North Highlands (black). The maximum 1-hour average value of the ground-based site (4.6) is colour-coded within the black frame; the corresponding satellite average is estimated to be 6.28 ± 2.72 .~~

4 Conclusions

We have performed an analysis of atmospheric carbon monoxide (CO) concentration changes introduced by emissions of fires using measurements in the shortwave infrared spectral range of the TROPOMI instrument onboard the Sentinel-5 Precursor satellite. The local CO emissions of Californian wildfires and subsequent transport can be clearly observed from space. ~~This is a demonstration of the unprecedented capabilities concerning level of detail modern wide-swath imaging satellite instruments~~

~~offer. As large sources are readily detected in a single overpass~~Due to its unique features, CO retrievals from TROPOMI have the potential to trigger model improvement and a better quantification of fire emissions by assimilation of the satellite-derived XCO in integrated systems such as CAMS.

Furthermore, new fields of application are enabled, in particular the detection of emission hot spots or air quality monitoring tasks~~. The assessment of the air quality~~ , because large sources are readily detected in a single overpass. The evaluation of TROPOMI's capabilities for dense air quality monitoring has shown that the quantitative assessment of the CO burden in Californian major cities ~~during the~~ is possible on a daily recurrent basis using the example of the first days of the Camp Fire and Woolsey Fire ~~can be thought of as an initial step in this direction.~~ in November 2018.

~~The analysed fires were the latest episodes of the deadliest and most destructive wildfire season the state of California has ever faced.~~ However, the accurate determination of boundary layer concentrations depends on reliable external mixing layer height information. In the case of fires, the feasibility is also subject to specific favourable circumstances affecting the vertical distribution of emissions. The local ambient atmospheric conditions such as stability and humidity have to ensure that most of the fire emissions stay within the boundary layer and that pyro-convection or direct injection to the free troposphere is unlikely. As a consequence, unknown plume dynamics remains the largest source of uncertainty in the calculation of the boundary layer CO burden caused by wildfires.

The quantitative analysis has shown that even intense wildfire events are not necessarily associated with the exceedance of national ambient air quality standards in the far field of the fires because all major city scenes for the analysed days comply with the regulatory limits. This finding is also confirmed by isolated ground-based air quality measurements near the most polluted city scenes.

Increasing unusual weather conditions with dryness of vegetation on the rise ~~bring deadly fires and associated air pollution forward. The increasing number of people living in the wildland-urban interface paired with proceeding climate change entailing~~ may lead to longer lasting and more intense fire seasons ~~temper the outlook for the future(Radeloff et al., 2018). Counter-measures with respect to forest management or building practices and mitigation of climate change will be key challenges of the century to prevent that fatal blazes and~~ in the future. Therefore, it is getting more and more important to monitor and forecast the air quality decline ~~establish as the new normal in the Western United States or other wildfire regions.~~ associated with wildfires in a changing climate to evaluate whether the compliance with regulatory limits will last or not. This can be achieved by an integrated monitoring system combining modelling with complementary information from accurate ground-based measurements and observations from various satellites.

Data availability. The carbon monoxide and methane data sets presented in this publication can be accessed via http://www.iup.uni-bremen.de/carbon_ghg/products/tropomi_wfmd/.

Author contributions. OS: writing the paper, design and operation of the satellite retrievals, data analysis, interpretation. MB, MR, HB, JPB: significant conceptual input to writing, design of the satellite retrievals, interpretation. All authors discussed the results and commented on the manuscript.

Competing interests. The authors declare that they have no conflict of interest.

Acknowledgements. ~~The research leading to these results has in part been funded by the ESA projects GHG-CCI and S5L2PP, the Federal Ministry of Education and Research project AIRSPACE, and by the State and the University of Bremen.~~

This publication contains modified Copernicus Sentinel data and modified Copernicus Climate Change Service Information (2018). Sentinel-5 Precursor is an ESA mission implemented on behalf of the European Commission. The TROPOMI payload is a joint development by ESA and the Netherlands Space Office (NSO). The Sentinel-5 Precursor ground-segment development has been funded by ESA and with national contributions from The Netherlands, Germany, and Belgium. The research leading to the presented results has in part been funded by the ESA projects GHG-CCI, GHG-CCI+, and S5L2PP, the Federal Ministry of Education and Research project AIRSPACE, and by the State and the University of Bremen.

We acknowledge the use of VIIRS imagery from the NASA Worldview application (https://worldview.earthdata.nasa.gov/) operated by the NASA/Goddard Space Flight Center Earth Science Data and Information System (ESDIS) project, the use of data from the California Department of Forestry and Fire Protection and the U.S. Environmental Protection Agency. We also thank the European Centre for Medium-Range Weather Forecasts (ECMWF) for providing the meteorological analysis~~and the~~, the ERA5 reanalysis, as well as the Copernicus Atmosphere Monitoring Service (CAMS) carbon monoxide ~~data~~analysis and Global Fire Assimilation System (GFAS) data. Neither the European Commission nor ECMWF is responsible for any use that may be made of the Copernicus Information or Data it contains. Ground-based CO data was obtained using the Air Quality Data (PST) Query Tool (https://www.arb.ca.gov/aqmis2/aqmis2.php) of the Air Quality and Meteorological Information System (AQMIS).

References

Bauduin, S., Clarisse, L., Theunissen, M., George, M., Hurtmans, D., Clerbaux, C., and Coheur, P.-F.: IASI's sensitivity to near-surface carbon monoxide (CO): Theoretical analyses and retrievals on test cases, J. Quant. Spectrosc. Radiat. Transfer, 189, 428–440, https://doi.org/10.1016/j.jqsrt.2016.12.022, 2017.

Bay Area Air Quality Management District: A Winter Spare the Air Alert is being called through Monday, November 12, due to smoke impacts from the Butte County fire, Press Release, November 9, http://www.baaqmd.gov/~/media/files/communications-and-outreach/publications/news-releases/2018/wsta_181109_2018_092-pdf.pdf, 2018.

Borsdorff, T., aan de Brugh, J., Hu, H., Hasekamp, O., Sussmann, R., Rettinger, M., Hase, F., Gross, J., Schneider, M., Garcia, O., Stremme, W., Grutter, M., Feist, D. G., Arnold, S. G., De Mazière, M., Kumar Sha, M., Pollard, D. F., Kiel, M., Roehl, C., Wennberg, P. O., Toon, G. C., and Landgraf, J.: Mapping carbon monoxide pollution from space down to city scales with daily global coverage, Atmos. Meas. Tech., 11, 5507–5518, https://doi.org/10.5194/amt-11-5507-2018, 2018a.

Borsdorff, T., Andrasec, J., aan de Brugh, J., Hu, H., Aben, I., and Landgraf, J.: Detection of carbon monoxide pollution from cities and wildfires on regional and urban scales: the benefit of CO column retrievals from SCIAMACHY 2.3 μm measurements under cloudy conditions, Atmos. Meas. Tech., 11, 2553–2565, https://doi.org/10.5194/amt-11-2553-2018, 2018b.

Bovensmann, H., Burrows, J. P., Buchwitz, M., Frerick, J., Noël, S., Rozanov, V. V., Chance, K. V., and Goede, A. P. H.: SCIAMACHY – Mission Objectives and Measurement Modes, J. Atmos. Sci., 56, 127–150, https://doi.org/10.1175/1520-0469(1999)056<0127:SMOAMM>2.0.CO;2, 1999.

Buchwitz, M., de Beek, R., Bramstedt, K., Noël, S., Bovensmann, H., and Burrows, J. P.: Global carbon monoxide as retrieved from SCIAMACHY by WFM-DOAS, Atmos. Chem. Phys., 4, 1945–1960, https://doi.org/10.5194/acp-4-1945-2004, 2004.

Buchwitz, M., de Beek, R., Noël, S., Burrows, J. P., Bovensmann, H., Schneising, O., Khlystova, I., Bruns, M., Bremer, H., Bergamaschi, P., Körner, S., and Heimann, M.: Atmospheric carbon gases retrieved from SCIAMACHY by WFM-DOAS: version 0.5 CO and CH_4 and impact of calibration improvements on CO_2 retrieval, Atmos. Chem. Phys., 6, 2727–2751, https://doi.org/10.5194/acp-6-2727-2006, 2006.

Buchwitz, M., Khlystova, I., Bovensmann, H., and Burrows, J. P.: Three years of global carbon monoxide from SCIAMACHY: comparison with MOPITT and first results related to the detection of enhanced CO over cities, Atmos. Chem. Phys., 7, 2399–2411, https://doi.org/10.5194/acp-7-2399-2007, 2007.

Burrows, J. P., Hölzle, E., Goede, A. P. H., Visser, H., and Fricke, W.: SCIAMACHY – Scanning Imaging Absorption Spectrometer for Atmospheric Chartography, Acta Astronautica, 35, 445–451, https://doi.org/10.1016/0094-5765(94)00278-T, 1995.

California Air Resources Board: Air Quality and Meteorological Information System, https://www.arb.ca.gov/aqmis2/aqmis2.php, 2018.

California Department of Forestry and Fire Protection: Statistics and Events, http://cdfdata.fire.ca.gov/incidents/incidents_statsevents, 2018.

Clerbaux, C., Boynard, A., Clarisse, L., George, M., Hadji-Lazaro, J., Herbin, H., Hurtmans, D., Pommier, M., Razavi, A., Turquety, S., Wespes, C., and Coheur, P.-F.: Monitoring of atmospheric composition using the thermal infrared IASI/MetOp sounder, Atmos. Chem. Phys., 9, 6041–6054, https://doi.org/10.5194/acp-9-6041-2009, 2009.

de Laat, A. T. J., Gloudemans, A. M. S., Aben, I., and Schrijver, H.: Global evaluation of SCIAMACHY and MOPITT carbon monoxide column differences for 2004–2005, J. Geophys. Res., 115, https://doi.org/10.1029/2009JD012698, 2010.

Deeter, M. N., Edwards, D. P., Gille, J. C., and Drummond, J. R.: Sensitivity of MOPITT observations to carbon monoxide in the lower troposphere, J. Geophys. Res., 112, https://doi.org/10.1029/2007JD008929, 2007.

Deeter, M. N., Martinez-Alonso, S., Andreae, M. O., and Schlager, H.: Satellite-Based Analysis of CO Seasonal and Interannual Variability Over the Amazon Basin, J. Geophys. Res., 123, 5641–5656, 2018.

Drummond, J. R., Zou, J., Nichitiu, F., Kar, J., Deschambaut, R., and Hackett, J.: A review of 9-year performance and operation of the MOPITT instrument, Adv. Space Res., 45, 760–774, https://doi.org/10.1016/j.asr.2009.11.019, 2010.

Eck, T. F., Holben, B. N., Reid, J. S., Sinyuk, A., Hyer, E. J., O'Neill, N. T., Shaw, G. E., Vande Castle, J. R., Chapin, F. S., Dubovik, O., Smirnov, A., Vermote, E., Schafer, J. S., Giles, D., Slutsker, I., Sorokine, M., and Newcomb, W. W.: Optical properties of boreal region biomass burning aerosols in central Alaska and seasonal variation of aerosol optical depth at an Arctic coastal site, J. Geophys. Res., 114, https://doi.org/10.1029/2008JD010870, 2009.

ECMWF: Part IV : Physical processes, IFS Documentation CY45R1, https://www.ecmwf.int/node/18714, 2018.

Field, R. D., van der Werf, G. R., Fanin, T., Fetzer, E. J., Fuller, R., Jethva, H., Levy, R., Livesey, N. J., Luo, M., Torres, O., and Worden, H. M.: Indonesian fire activity and smoke pollution in 2015 show persistent nonlinear sensitivity to El Niño-induced drought, Proc. Natl. Acad. Sci. USA, 113, 9204–9209, https://doi.org/10.1073/pnas.1524888113, 2016.

Fromm, M., Lindsey, D. T., Servranckx, R., Yue, G., Trickl, T., Sica, R., Doucet, P., and Godin-Beekmann, S.: The Untold Story of Pyrocumulonimbus, Bulletin of the American Meteorological Society, 91, 1193–1210, https://doi.org/10.1175/2010BAMS3004.1, 2010.

Fu, Y., Li, R., Huang, J., Bergeron, Y., Fu, Y., Wang, Y., and Gao, Z.: Satellite-Observed Impacts of Wildfires on Regional Atmosphere Composition and the Shortwave Radiative Forcing: A Multiple Case Study, J. Geophys. Res., 123, 8326–8343, 2018.

Hersbach, H., de Rosnay, P., Bell, B., Schepers, D., Simmons, A., Soci, C., Abdalla, S., Alonso-Balmaseda, M., Balsamo, G., Bechtold, P., Berrisford, P., Bidlot, J.-R., de Boisséson, E., Bonavita, M., Browne, P., Buizza, R., Dahlgren, P., Dee, D., Dragani, R., Diamantakis, M., Flemming, J., Forbes, R., Geer, A. J., Haiden, T., Hólm, E., Haimberger, L., Hogan, R., Horányi, A., Janiskova, M., Laloyaux, P., Lopez, P., Munoz-Sabater, J., Peubey, C., Radu, R., Richardson, D., Thépaut, J.-N., Vitart, F., Yang, X., Zsótér, E., and Zuo, H.: Operational global reanalysis: progress, future directions and synergies with NWP, ERA Report Series, https://doi.org/10.21957/tkic6g3wm, 2018.

Hillger, D., Seaman, C., Liang, C., Miller, S., Lindsey, D., and Kopp, T.: Suomi NPP VIIRS Imagery evaluation, J. Geophys. Res.: Atmospheres, 119, 6440–6455, https://doi.org/10.1002/2013JD021170, 2014.

Hutchison, K. D. and Cracknell, A. P.: Visible Infrared Imager Radiometer Suite: A New Operational Cloud Imager, CRC Press of Taylor and Francis, London, 2005.

Inness, A., Blechschmidt, A.-M., Bouarar, I., Chabrillat, S., Crepulja, M., Engelen, R. J., Eskes, H., Flemming, J., Gaudel, A., Hendrick, F., Huijnen, V., Jones, L., Kapsomenakis, J., Katragkou, E., Keppens, A., Langerock, B., de Mazière, M., Melas, D., Parrington, M., Peuch, V. H., Razinger, M., Richter, A., Schultz, M. G., Suttie, M., Thouret, V., Vrekoussis, M., Wagner, A., and Zerefos, C.: Data assimilation of satellite-retrieved ozone, carbon monoxide and nitrogen dioxide with ECMWF's Composition-IFS, Atmos. Chem. Phys., 15, 5275–5303, https://doi.org/10.5194/acp-15-5275-2015, 2015.

Kaiser, J. W., Heil, A., Andreae, M. O., Benedetti, A., Chubarova, N., Jones, L., Morcrette, J.-J., Razinger, M., Schultz, M. G., Suttie, M., and van der Werf, G. R.: Biomass burning emissions estimated with a global fire assimilation system based on observed fire radiative power, Biogeosciences, 9, 527–554, https://doi.org/10.5194/bg-9-527-2012, 2012.

Labonne, M., Bréon, F.-M., and Chevallier, F.: Injection height of biomass burning aerosols as seen from a spaceborne lidar, Geophys. Res. Lett., 34, https://doi.org/10.1029/2007GL029311, 2007.

Luo, M., Shephard, M. W., Cady-Pereira, K. E., Henze, D. K., Zhu, L., Bash, J. O., Pinder, R. W., Capps, S. L., Walker, J. T., and Jones, M. R.: Satellite observations of tropospheric ammonia and carbon monoxide: Global distributions, regional correlations and comparisons to model simulations, Atmospheric Environment, 106, 262–277, https://doi.org/https://doi.org/10.1016/j.atmosenv.2015.02.007, 2015.

Mazzoni, D., Logan, J. A., Diner, D., Kahn, R., Tong, L., and Li, Q.: A data-mining approach to associating MISR smoke plume heights with MODIS fire measurements, Remote Sensing of Environment, 107, 138–148, https://doi.org/10.1016/j.rse.2006.08.014, 2007.

McMillan, W. W., Barnet, C., Strow, L., Chahine, M. T., McCourt, M. L., Warner, J. X., Novelli, P. C., Korontzi, S., Maddy, E. S., and Datta, S.: Daily global maps of carbon monoxide from NASA's Atmospheric Infrared Sounder, Geophys. Res. Lett., 32, https://doi.org/10.1029/2004GL021821, 2005.

Omaye, S. T.: Metabolic modulation of carbon monoxide toxicity, Toxicology, 180, 139–150, https://doi.org/10.1016/S0300-483X(02)00387-6, 2002.

Radeloff, V. C., Helmers, D. P., Kramer, H. A., Mockrin, M. H., Alexandre, P. M., Bar-Massada, A., Butsic, V., Hawbaker, T. J., Martinuzzi, S., Syphard, A. D., and Stewart, S. I.: Rapid growth of the US wildland-urban interface raises wildfire risk, Proc. Natl. Acad. Sci. USA, 115, 3314–3319, https://doi.org/10.1073/pnas.1718850115, 2018.

Radke, L. F., Lyons, J. H., Hobbs, P. V., Hegg, D. A., Sandberg, D. V., and Ward, D. E.: Airborne Monitoring and Smoke Characterization of Prescribed Fires on Forest Lands in Western Washington and Oregon: Final Report, United States Department of Agriculture, Forest Service, General Technical Report PNW-GTR-251, https://www.fs.fed.us/pnw/pubs/gtr251.pdf, 1990.

Sacramento Metropolitan Air Quality Management District: Smoke Health Statement Due to Camp Fire, Press Release, November 9, http://www.airquality.org/Communications/Documents/SmokeHealthStatement_CampFire_110918_2.docx.pdf, 2018.

Schneising, O.: Sentinel-5 Precursor methane: Retrieval, comparisons and interpretation (S5PCH4), Technical Report ESA project GHG-CCI, 2017.

Schneising, O., Buchwitz, M., Burrows, J. P., Bovensmann, H., Reuter, M., Notholt, J., Macatangay, R., and Warneke, T.: Three years of greenhouse gas column-averaged dry air mole fractions retrieved from satellite - Part 1: Carbon dioxide, Atmos. Chem. Phys., 8, 3827–3853, https://doi.org/10.5194/acp-8-3827-2008, 2008.

Schneising, O., Buchwitz, M., Reuter, M., Heymann, J., Bovensmann, H., and Burrows, J. P.: Long-term analysis of carbon dioxide and methane column-averaged mole fractions retrieved from SCIAMACHY, Atmos. Chem. Phys., 11, 2863–2880, https://doi.org/10.5194/acp-11-2863-2011, 2011.

Schneising, O., Burrows, J. P., Dickerson, R. R., Buchwitz, M., Reuter, M., and Bovensmann, H.: Remote sensing of fugitive methane emissions from oil and gas production in North American tight geologic formations, Earth's Future, 2, 548–558, https://doi.org/10.1002/2014EF000265, 2014.

Schneising, O., Buchwitz, M., Reuter, M., Bovensmann, H., Burrows, J. P., Borsdorff, T., Deutscher, N. M., Feist, D. G., Griffith, D. W. T., Hase, F., Hermans, C., Iraci, L. T., Kivi, R., Landgraf, J., Morino, I., Notholt, J., Petri, C., Pollard, D. F., Roche, S., Shiomi, K., Strong, K., Sussmann, R., Velazco, V. A., Warneke, T., and Wunch, D.: A scientific algorithm to simultaneously retrieve carbon monoxide and methane from TROPOMI onboard Sentinel-5 Precursor, Atmos. Meas. Tech. Discuss., 2019, 1–44, in review, https://doi.org/10.5194/amt-2019-243, 2019.

Shettle, E. P. and Fenn, R. W.: Models for the aerosols of the lower atmosphere and the effects of humidity variations on their optical properties, Environmental Research Papers, Optical Physics Division, Air Force Geophysics Laboratory, MA, 1979.

Sofiev, M., Ermakova, T., and Vankevich, R.: Evaluation of the smoke-injection height from wild-land fires using remote-sensing data, Atmos. Chem. Phys., 12, 1995–2006, https://doi.org/10.5194/acp-12-1995-2012, 2012.

Stith, J. L., Radke, L. F., and Hobbs, P. V.: Particle emissions and the production of ozone and nitrogen oxides from the burning of forest slash, Atmospheric Environment, 15, 73–82, https://doi.org/https://doi.org/10.1016/0004-6981(81)90127-X, 1981.

Swain, D. L., Horton, D. E., Singh, D., and Diffenbaugh, N. S.: Trends in atmospheric patterns conducive to seasonal precipitation and temperature extremes in California, Science Advances, 2, e1501344, https://doi.org/10.1126/sciadv.1501344, 2016.

The Royal Society: Ground-level ozone in the 21st century: future trends, impacts and policy implications, Science Policy Report 15/08, https://royalsociety.org/~/media/Royal_Society_Content/policy/publications/2008/7925.pdf, 2008.

Tosca, M. G., Randerson, J. T., Zender, C. S., Nelson, D. L., Diner, D. J., and Logan, J. A.: Dynamics of fire plumes and smoke clouds associated with peat and deforestation fires in Indonesia, J. Geophys. Res., 116, https://doi.org/10.1029/2010JD015148, 2011.

Turquety, S., Hurtmans, D., Hadji-Lazaro, J., Coheur, P.-F., Clerbaux, C., Josset, D., and Tsamalis, C.: Tracking the emission and transport of pollution from wildfires using the IASI CO retrievals: analysis of the summer 2007 Greek fires, Atmos. Chem. Phys., 9, 4897–4913, https://doi.org/10.5194/acp-9-4897-2009, 2009.

United States Geological Survey: Land Cover Products – Global Land Cover Characterization (GLCC), https://doi.org/10.5066/F7GB230D, https://www.usgs.gov/centers/eros/science/usgs-eros-archive-land-cover-products-global-land-cover-characterization-glcc, 2018.

U.S. Environmental Protection Agency: National Ambient Air Quality Standards (NAAQS) for Carbon Monoxide (CO), Federal Register: 76 FR 54293, http://www.gpo.gov/fdsys/pkg/FR-2011-08-31/pdf/2011-21359.pdf, 2011.

Van Roozendael et al.: Sentinel 5 L2 Prototype Processors: Scientific Verification Report, Technical Report ESA project S5L2PP, 2018.

Veefkind, J. P., Aben, I., McMullan, K., Förster, H., de Vries, J., Otter, G., Claas, J., Eskes, H. J., de Haan, J. F., Kleipool, Q., van Weele, M., Hasekamp, O., Hoogeveen, R., Landgraf, J., Snel, R., Tol, P., Ingmann, P., Voors, R., Kruizinga, B., Vink, R., Visser, H., and Levelt, P. F.: TROPOMI on the ESA Sentinel-5 Precursor: A GMES mission for global observations of the atmospheric composition for climate, air quality and ozone layer applications, Remote Sensing of Environment, 120, 70–83, https://doi.org/10.1016/j.rse.2011.09.027, 2012.

Worden, H. M., Deeter, M. N., Edwards, D. P., Gille, J. C., Drummond, J. R., and Nédélec, P.: Observations of near-surface carbon monoxide from space using MOPITT multispectral retrievals, J. Geophys. Res., 115, D18314, https://doi.org/10.1029/2010JD014242, 2010.

World Health Organization: Air quality guidelines global update 2005 : particulate matter, ozone, nitrogen dioxide and sulfur dioxide, https://apps.who.int/iris/handle/10665/107823, 2006.

Wunch, D., Toon, G. C., Blavier, J.-F. L., Washenfelder, R. A., Notholt, J., Connor, B. J., Griffith, D. W. T., Sherlock, V., and Wennberg, P. O.: The Total Carbon Column Observing Network, Phil. Trans. R. Soc. A, 369, 2087–2112, https://doi.org/10.1098/rsta.2010.0240, 2011.

Yurganov, L. N., Duchatelet, P., Dzhola, A. V., Edwards, D. P., Hase, F., Kramer, I., Mahieu, E., Mellqvist, J., Notholt, J., Novelli, P. C., Rockmann, A., Scheel, H. E., Schneider, M., Schulz, A., Strandberg, A., Sussmann, R., Tanimoto, H., Velazco, V., Drummond, J. R., and Gille, J. C.: Increased Northern Hemispheric carbon monoxide burden in the troposphere in 2002 and 2003 detected from the ground and from space, Atmos. Chem. Phys., 5, 563–573, https://doi.org/10.5194/acp-5-563-2005, 2005.